

# Operator-Based Truncation Scheme Based on the Many-Body Fermion Density Matrix

Siew-Ann Cheong and Christopher L. Henley  
*Laboratory of Atomic and Solid State Physics, Cornell University*  
(Dated: May 28, 2018)

In an earlier work [S. A. Cheong and C. L. Henley, cond-mat/0206196 (2002)], we derived an exact formula for the many-body density matrix  $\rho_B$  of a block of  $B$  sites cut out from an infinite chain of noninteracting spinless fermions, and found that the many-particle eigenvalues and eigenstates of  $\rho_B$  can all be constructed out of the one-particle eigenvalues and one-particle eigenstates respectively. In this paper we improved upon this understanding, and developed a statistical-mechanical analogy between the density matrix eigenstates and the many-body states of a system of noninteracting fermions. Each density matrix eigenstate corresponds to a particular set of occupation of single-particle pseudo-energy levels, and the density matrix eigenstate with the largest weight, having the structure of a Fermi sea ground state, unambiguously defines pseudo-Fermi level. Based on this analogy, we outlined the main ideas behind an operator-based truncation of the density matrix eigenstates, where single-particle pseudo-energy levels far away from the pseudo-Fermi level are removed as degrees of freedom. We report numerical evidence for scaling behaviours in the single-particle pseudo-energy spectrum for different block sizes  $B$  and different filling fractions  $\bar{n}$ . With the aid of these scaling relations, which tells us that the block size  $B$  plays the role of an inverse temperature in the statistical-mechanical description of the density matrix eigenstates and eigenvalues, we looked into the performance of our operator-based truncation scheme in minimizing the discarded density matrix weight and the error in calculating the dispersion relation for elementary excitations. This performance was compared against that of the traditional density matrix-based truncation scheme, as well as against a operator-based plane wave truncation scheme, and found to be very satisfactory.

## I. INTRODUCTION

An unsolved problem in many-body physics is to augment numerical exact diagonalization, which is only feasible on comparatively small systems, so as to give the maximum information about the thermodynamic limit. We know from the renormalization group that only a few degrees of freedom, *viz.* those with low energies and long wavelengths, really matter. Hence it should be possible in principle to discard the irrelevant parts of the Hilbert space, but no method has been developed in real space for higher-dimensional, interacting lattice models. The density matrix renormalization group (DMRG)<sup>1-4</sup> is the only successful method to date, but it is limited to one-dimensional chains, or two-dimensional systems that can be forced into one dimension as strips.<sup>5,6</sup>

To get more mileage out of density matrix-based renormalization group methods, surely we must develop a deep understanding of the structure of density matrices of the simplest possible systems, for which analytic results are available to guide us. Therefore, it is appropriate to begin by considering the ground state of a one-dimensional chain of noninteracting spinless fermions described by a nearest-neighbour hopping Hamiltonian

$$H = - \sum_j [c_j^\dagger c_{j+1} + c_{j+1}^\dagger c_j]. \quad (1.1)$$

Here we observe that, in one dimension, one has the same

Fermi sea ground state for a variety of translationally-invariant Hamiltonians with hoppings to further neighbors, provided their dispersion relation is monotonic so that the Fermi surface occurs at the same wavevector for a given filling. A ‘block’ is then identified within this one-dimensional system by choosing  $B$  sites that need not be contiguous, following which we can define the many-body density matrix  $\rho_B$  of the block starting from the zero-temperature many-body wavefunction and tracing out all sites outside the chosen block of  $B$  sites. The basis of this paper is the simple factorized nature of  $\rho_B$  and its eigenfunctions, which we derived exactly for noninteracting (spinless or spinfull) fermions,<sup>7</sup> by extending a technique introduced by Chung and Peschel.<sup>8</sup>

In Ref.8, it was shown that many-particle density matrix eigenstates are built from a set of single-particle creation operators and eigenvalues, quite analogous to the energy eigenstates of a noninteracting system of fermions. For a block of  $B$  sites cut out from a larger overall system, there are  $B$  such *pseudo-creation operators*  $f_l^\dagger$ , and the block’s Hilbert space is therefore spanned by all  $2^B$  products of the  $f_l^\dagger$ ’s. The density matrix of the block can be written as

$$\rho_B = \mathcal{Q}^{-1} \exp(-\tilde{H}), \quad (1.2)$$

which is the exponential of a *pseudo-Hamiltonian* given

by

$$\tilde{H} = \sum_{l=1}^B \varphi_l f_l^\dagger f_l, \quad (1.3)$$

with *single-particle pseudo-energy spectrum*  $\varphi_l$ .

This paper is devoted entirely to noninteracting fermions, because the analytic results of Ref.7 permit many calculations that could not be done by numerical brute force in an interacting case, or can be carried out only by quite different methods (such as Monte Carlo). Furthermore, our hypothetical renormalization or projection algorithm using DM truncation would first be applied to a well-understood system in which the low-energy excitations behave as noninteracting quasiparticles (as in a Fermi liquid or a  $d$ -wave superconducting phase). Our imagined numerical method in such a system would extract renormalized pseudo-creation operators  $\tilde{f}_l^\dagger$  which are related to the single-particle operators  $\{f_l^\dagger\}$  in the same way that quasiparticle creation operators are related to bare fermion creation operators. The pseudo-dispersion relation for the renormalized  $\{\tilde{f}_l^\dagger\}$  is thus expected to scale in the same fashion as the pseudo-dispersion  $\varphi_l$  encoded in (1.3) of the noninteracting fermions considered in this paper.

Through the calculations in this paper we aim to understand the analytic structure of  $\rho_B$ , and to begin to understand the quantitative errors due to truncation. This includes the question: what is the proper measure of error? The most familiar measure, the retained fraction of total density matrix weight, does not seem to be the best measure of error, as evidenced by the small errors obtained in Section VI for the calculations of the dispersion relation. Another question to be investigated is whether — when we are severely truncating the Hilbert space, and attempting only to obtain the low-energy excitations — the density matrix eigenstates are the optimal basis. As shown by the comparison in Section VII, they are certainly superior to the other plausible basis (plane waves).

In Section II A, we summarize first our much improved understanding of the analytic structure of the density matrix for noninteracting fermions (and by implication for any Fermi liquid) following from (1.2) and (1.3), and elucidate the statistical-mechanical analogy between the density matrix eigenstates and the many-body states of a system of noninteracting spinless fermions. In Section II B, we summarize the important results which we obtained in Ref.7, giving exact relationships between the block density matrix  $\rho_B$ , the Green function matrix  $G$  restricted to the block, as well as their eigenstates and eigenvalues. Then in Section II C, we develop the main ideas behind a *operator-based density matrix (DM) truncation scheme* based on the statistical-mechanical analogy described in Section II A.

The relation between the single-particle density matrix eigenstates and single-particle energy eigenstates of a sys-

tem of noninteracting spinless fermions also suggests how the distribution of single-particle pseudo-energies  $\varphi_l$  are expected to scale with the block size  $B$ . Numerically, a scaling relationship between  $\varphi_l$  and  $B$  was found indeed, for the overall chain at various fillings  $\bar{n}$ . Our analytical results from Ref.7 shed light on this eigenvalue scaling in two ways. Firstly, as in Ref.8, they allow numerical study of the density matrix for system sizes so large that they would be inaccessible to any other techniques. Secondly, the exact connection of the block density matrix  $\rho_B$  to the block Green function matrix  $G$  gives hints about the eigenvalue distribution. All of these will be discussed further in Section III, and the implications of the scaling behaviour of the single-particle pseudo-energies are discussed in Section IV, where we derived the asymptotic behaviour, in the limit of infinite block sizes, of the largest density matrix weight and the truncated weight  $W_t$ , which is the sum of weights of the density matrix eigenstates retained in the operator-based DM truncation scheme.

Compared to the traditional density matrix truncation scheme used in the DMRG, our operator-based density matrix truncation scheme gives for the same number of density matrix eigenstates retained a slightly larger discarded weight  $\epsilon = 1 - W_t$  (see FIG. 8 in Section IV D). This quantity gives a  $O(\epsilon)$  estimate as an upper bound — a worst case scenario — for the error incurred when computing the expectation of a most general observable. As with examples in numerical integration, the performance of an algorithm in integrating some classes of functions may be much better than that expected from the straightforward error analysis. In any case, we are not really interested in arbitrary observables, but rather, in the dispersion relation of elementary excitations, which we calculate in Section VI. The results are highly encouraging: the dispersion relation calculated in the operator-based DM truncation scheme differ from the true dispersion relation by an amount much smaller than what is suggested by the discarded weight.

Besides quasiparticle dispersion relations, real space correlation functions are also interesting quantities to calculate, and these invariably depend on the real space structure of the many-body ground state wavefunction. Since this wavefunction is to be written in terms of the one-particle density matrix eigenfunctions, it is important to understand the real space structure of these as well. The one-particle density matrix eigenfunctions kept in our operator-based DM truncation scheme have spatial structures that are very similar to each other. In Section V we look into a representative one-particle density matrix eigenfunction, the pseudo-Fermi eigenfunction, for each  $B$ , and found that they also obey a universal scaling relation. Then in Section VI C, we check how well such a truncated basis of one-particle density matrix eigenfunctions can approximate the true single-particle wavefunction at the Fermi level, which is a plane wave with wavevector  $k_F$ . We find the approximation to be

good even when less than one quarter of the one-particle density matrix eigenfunctions are kept. This is impressive, considering the fact that in the operator-based DM truncation scheme, the number of many-particle density matrix eigenstates thus represented by the one-particle density matrix eigenstates retained constitutes a miniscule fraction of the total number of density matrix eigenstates.

Finally, for systems where we know that the true single-particle wavefunctions are plane waves, it seems *a priori* plausible that a plane wave-based operator-based truncation scheme might outperform the operator-based density matrix truncation scheme. We look into this possibility in Section VII, and find that while there are a few aspects in calculating the dispersion relation where the *operator-based plane wave (PW) truncation scheme* outperforms the operator-based DM truncation scheme, the overall performance of the PW scheme is inferior to the DM scheme. We then conclude in Section VIII by summarizing the important results obtained in this paper, and discuss where all these might fit into the numerical analysis of an interacting system.

## II. OPERATOR-BASED DENSITY MATRIX TRUNCATION

### A. Structure of Density Matrix Eigenvalues and Eigenstates

Because the Hamiltonian in (1.1) conserves particle number, the eigenstates of  $\rho_B$  have definite particle number, and may be grouped into various  $P$ -particle sectors, where  $P = 0, 1, \dots, B$ . A consequence of our fundamental formulas (1.2) and (1.3) is that every eigenstate of  $\rho_B$  has the form

$$|\chi_L\rangle = \prod_{p=1}^P f_{l_p}^\dagger |0\rangle. \quad (2.1)$$

Each eigenstate is specified by a list of *pseudo-occupation numbers*  $\{n_l\}$ , where  $n_{l_p} = 1$  for the factors contained in (2.1), and is zero otherwise. Furthermore, the corresponding eigenvalue, the *density matrix weight*, is simply given by

$$w_L = \mathcal{Q}^{-1} \exp \left[ - \sum_{l=1}^B n_l \varphi_l \right], \quad (2.2)$$

where the quantity

$$\Phi = \sum_l n_l \varphi_l \quad (2.3)$$

appearing in the exponent is the *total pseudo-energy*. In terms of the single-particle pseudo-energies  $\{\varphi_l\}$ , the normalization constant of the density matrix in (1.2) can be

written as

$$\mathcal{Q} \equiv \sum_{\{n_l\}} \exp \left[ - \sum_l n_l \varphi_l \right], \quad (2.4)$$

where the summation is over all  $2^B$  combinations of occupations.

It is immediately clear from (2.2) that the density matrix eigenstate of maximum weight corresponds to the minimum total pseudo-energy. This is obtained by setting  $n_l = 1$  for  $\varphi_l < 0$  and  $n_l = 0$  for  $\varphi_l > 0$ . In complete analogy to the real energy of a noninteracting system of fermions, we simply fill up the *single-particle pseudo-energy levels (PELs)* from the lowest up to a *pseudo-Fermi level*. The maximum density matrix weight always turns out to occur with the block fractional filling that is closest to the bulk filling of the Fermi sea ground state. More generally, the maximum-weight state in the  $P$ -particle sector is obtained by filling the states with the  $P$  lowest single-particle pseudo-energies. Finally, it is clear that the next-highest weights, or equivalently the next-lowest total pseudo-energies in the  $P$ -particle sector, are obtained by making particle-hole excitations involving the PELs near to the last one filled.

The above analogy may be extended to note that (1.2) is exactly the density matrix that would be obtained (see for example, Ref.9) at temperature  $T = 1$  if  $\tilde{H}$  were the Hamiltonian. The reciprocal of the normalization constant  $\mathcal{Q}$  of  $\rho_B$  in (2.4) just corresponds to the grand partition function for the block of  $B$  sites. Among other things, this implies that  $\langle n_l \rangle$ , the average particle number in a particular PEL, has the functional form of the Fermi-Dirac distribution.

We will actually apply this idea in a slightly different way, so as to relate the single-particle pseudo-energies  $\varphi_l$  for different block sizes. If we were dealing with an actual Hamiltonian, the dispersion relation would imply a density of states which would be multiplied by the system size to obtain the actual distribution of states. Our numerical scaling results in Section III A confirm that pseudo-energies behave similarly to real energies.

### B. Relation of Pseudo-Energies to Block Green Function Matrix

In our earlier work<sup>7</sup> we obtain an exact formula

$$\tilde{H} = - \sum_{ij} [\log_e G(\mathbb{1} - G)^{-1}]_{ij} c_i^\dagger c_j, \quad (2.5)$$

which, with (1.2), relates  $\rho_B$  to the block Green function matrix  $G$ , whose matrix elements are  $G_{ij} = \langle c_i^\dagger c_j \rangle$  with  $i$  and  $j$  restricted to sites within the block. Clearly (2.5) becomes (1.2) when the pseudo-Hamiltonian is diagonalized. Also, (2.5) tells us that the quadratic form of  $\tilde{H}$

in (2.5) and  $G$  are simultaneously diagonalizable. If we denote by

$$|\chi_l\rangle = f_l^\dagger |0\rangle = \sum_{j=1}^B \chi_l(j) c_j^\dagger |0\rangle, \quad (2.6)$$

the single-particle eigenstate of  $\tilde{H}$  with eigenvalue  $\varphi_l$ , then  $\{\chi_l(j)\}$  is the eigenvector of  $G$  with eigenvalue  $\lambda_l$ . The single-particle pseudo-energies are related to the eigenvalues of  $G$  by

$$\varphi_l = -\log_e \frac{\lambda_l}{1 - \lambda_l}, \quad (2.7)$$

or equivalently,

$$\lambda_l = \frac{1}{\exp \varphi_l + 1}, \quad (2.8)$$

i.e. the eigenvalues of  $G$  are the average pseudo-occupation numbers  $\langle n_l \rangle$ . Note that we sometimes write  $\varphi_l \rightarrow \varphi(l, B)$  to make explicit the dependence on block size  $B$ . We will assume that  $\varphi_l$  are ordered from the most negative to the most positive values.

Another notable result that was derived in Ref.7 is that

$$\mathcal{Q}^{-1} = \det(\mathbb{1} - G) = \prod_{l=1}^B (1 - \lambda_l). \quad (2.9)$$

Along with (2.5) and (2.7), (2.9) comprises the final ingredients that allow numerical computation of the density matrix even in very large blocks. Aside from the possibilities of truncation, (2.1) through (2.9) have completely reduced a  $2^B \times 2^B$  diagonalization problem into a  $B \times B$  problem, a computational shortcut which allows numerical studies of large blocks.

### C. Recipe for Operator-Based Truncation

The analytical structure of (1.3) hints at the proper design of a truncation scheme. The retained Hilbert space of a block *should not* be the span of those density matrix eigenstates whose weight exceeds a cutoff. Instead, we should implement a ‘consistent’ truncation, such that the truncated Hilbert space consists of exactly  $2^{l_{\max}}$  states, built from all combinations of  $l_{\max}$  pseudo-creation operators  $f_1^\dagger, \dots, f_{l_{\max}}^\dagger$ , acting on a block ‘vacuum state’  $|0\rangle_B$ , and satisfying fermion anticommutation relations.

In the traditional density matrix-based truncation scheme used in DMRG, the recipe for truncation is to sort all density matrix weights in descending order, and then retain only the eigenstates associated with the weights that exceed a certain cut off. Let us refer to this as the *weight-ranked DM truncation scheme*. In light of our understanding of the structure of the many-body density matrix presented in this paper, we can see that the

weight-ranked DM truncation scheme will certainly retain the eigenstate with maximum weight, the pseudo-Fermi sea described in Section II A, along with eigenstates that are ‘particle excitations’, ‘hole excitations’ and ‘particle-hole excitations’ from the pseudo-Fermi sea. If we arrange the entire collection of many-particle density matrix eigenstates into a state graph, then the state graph looks like a  $B$ -dimensional hypercubic lattice near the pseudo-Fermi sea. What the weight-ranked DM truncation does in this state graph picture is to remove nodes, and in effect cut bonds, out from this hypercubic lattice, producing a subgraph that is much less connected and containing tenuous links. Because of this, when the Hamiltonian is projected onto the weight-ranked DM truncated basis, spurious interactions are introduced.

We can apply the pseudo-energy analogy in choosing how to truncate, given the form of the density matrix. It is familiar, in the truncation used in Fourier-space-based quantum renormalization groups, to discard all single-particle degrees of freedom except for a shell around the Fermi surface. In the same way, let us discard all operators  $f_l$  as degrees of freedom, except those for which  $|\varphi_l|$  is less than some threshold  $\varphi_*$ . For all other  $f_l$ , we ‘freeze’  $n_l$  by setting  $n_l$  to its ground state value

$$n_l = \begin{cases} 1, & \text{for } \varphi_l < -\varphi_*; \\ 0, & \text{for } \varphi_l > \varphi_*. \end{cases} \quad (2.10)$$

This choice gives the maximum density matrix weight, among the eigenstates having any particular set of  $n_l$  for the retained single-particle pseudo-energy levels. The spirit of this truncation scheme is similar to that used in quantum chemistry,<sup>10–12</sup> except that the notion of a Fermi surface is more fuzzy in atoms and molecules. The idea that truncation consists of decreasing the thickness of a shell of wavevectors around the Fermi surface appeared in the original renormalization group for a quantum-mechanical solid-state problem (Anderson’s poor man’s RG for the Kondo problem).<sup>13</sup> This obvious notion — that the action is around the Fermi surface — necessarily appears in every effective form of truncation intended for a metal (see for example, Ref.14 and Ref.15, among others). However, to our knowledge all such schemes used a basis of plane waves or of energy eigenstates. Our variation uses PELs in analogy to the use of energy eigenstates in these previous problems. Deriving from the density matrix, it makes sense only in procedures that involving cutting a real-space block out of a larger system.

Within this *operator-based density matrix (DM) truncation scheme*, we can define an effective Hamiltonian for the truncated Hilbert space, just by taking the matrix elements of the true Hamiltonian between all the retained states. Using an operator-based truncation, this will have a particularly clean form: first replace each creation operator  $c_j^\dagger$  by the equivalent combination of all  $\{f_l^\dagger\}$ ; then replace  $f_l^\dagger f_l \rightarrow 1$  for each single-particle pseudo-energy

$\varphi_l < -\varphi_*$  (these are frozen to be always occupied), and otherwise remove all terms involving the operators that are truncated. Thus, if the original Hamiltonian has at most  $l_{\max}$ -fermion terms, the same will be true for the truncated Hamiltonian. This prescription shows that such a truncation is possible for general models, once one knows the appropriate density matrix, but in this paper we have applied it only to noninteracting models.

### III. SCALING BEHAVIOUR OF EIGENVALUE DISTRIBUTION

Since the many-particle density matrix eigenvalues are built, according to (2.2), from the single-particle pseudo-energies, the latter are the focus of our numerical investigations. Now if our entire system consisted of the block in a pure state at  $T = 0$ , then every eigenvalue  $\lambda_l$  of the block Green function matrix  $G$ , being the average pseudo-occupation number  $\langle n_l \rangle$  of a PEL, would either be one or zero. At  $T > 0$ ,  $\lambda_l$  follow a Fermi-Dirac distribution. We will see later that cutting out a finite block from a  $T = 0$  system, by tracing over the environment of the block, has a similar effect on the eigenvalues of  $G$  as would taking  $T > 0$  when the block is the whole system.

In a translationally invariant system with filling  $\bar{n}$  (at  $T = 0$ ), a fraction  $\bar{n}$  of the eigenvalues of  $G$  are one, while the rest are zero. Cutting out a block of length  $B$  must smooth out this step (much as having  $T > 0$  makes it into a Fermi-Dirac distribution), and we expect the transition from one to zero to occur over a fraction  $\sim 1/B$ . This guess was inspired by the analogy of pseudo-energy  $\varphi_l$  in (1.3) to the real energy, which near the Fermi level scales linearly with wavevector  $\sim 1/B$ . This  $B^{-1}$  scaling suggests the conjecture of a scaling form for the single-particle pseudo-energy like  $\varphi_l \approx Bf(l/B)$ , and indeed we find below just such a scaling form.

#### A. Pseudo-Energies and Pseudo-Occupation Numbers

In this subsection we calculate numerically the eigenvalues  $\lambda_l$  of the block Green function matrix  $G$ , and use (2.7) to compute the single-particle pseudo-energies  $\varphi_l$ . For a chain of free spinless fermions in its ground state, the matrix elements of the block Green function matrix  $G$  are

$$G_{ij} = \frac{\sin \pi \bar{n} |i - j|}{\pi |i - j|}, \quad (3.1)$$

where  $\bar{n}$  is the filling fraction. FIG. 1 shows how  $\lambda_l$ , the eigenvalues of  $G$ , are distributed for different filling fractions  $\bar{n}$  and different block sizes  $B$ .

For  $\bar{n} = \frac{1}{2}$ , our numerical studies suggest a scaling relationship of the form

$$\varphi(l, B) \cong Bf(x), \quad (3.2)$$

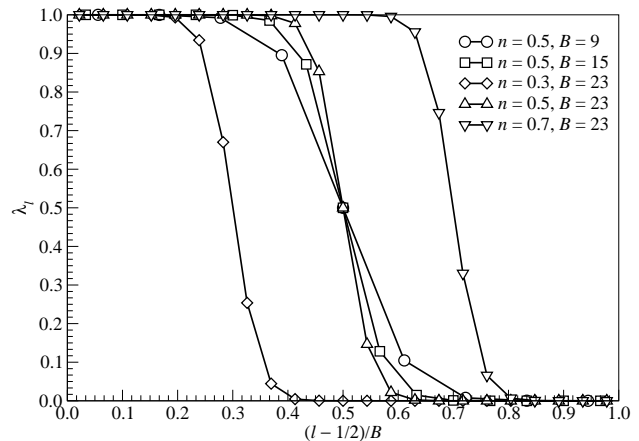


FIG. 1: Distribution of  $\lambda_l$  for different filling fractions and block sizes. In order to compare  $\lambda_l$  for different block sizes, the interval  $l \in [1, B]$  is rescaled such that  $(l - \frac{1}{2})/B \in (0, 1)$ . With this rescaling,  $\lambda = \frac{1}{2}$  always occur at  $[(l - \frac{1}{2})/B] = \bar{n}$ .

where  $x \equiv [(l - \frac{1}{2})/B] - \frac{1}{2}$ , as shown in FIG. 2. There are two points on FIG. 2 we would like to note. First of all, with our choice of the scaling variable  $x$ , the scaling function  $f(x)$  always passes through the origin, i.e.

$$f(0) = 0. \quad (3.3)$$

Secondly, from FIG. 2, we see that  $f(x)$  is an odd function, i.e.

$$f(-x) = -f(x), \quad (3.4)$$

which is what we would expect from particle-hole symmetry when the overall system is at half-filling, and  $f(x)$  has a finite positive slope at  $x = 0$ , i.e.

$$f'(0) > 0. \quad (3.5)$$

Similar scaling behaviours of the form

$$\varphi(l, B, \bar{n}) \cong Bf(\bar{n}, x) \quad (3.6)$$

are found for all  $\bar{n}$ , with the generic scaling variable

$$x \equiv (l - l_F)/B, \quad (3.7)$$

where

$$l_F = \bar{n}B + \frac{1}{2} \quad (3.8)$$

plays the role of a Fermi wavevector, and a filling fraction-dependent scaling function  $f(\bar{n}, x)$ , as shown in FIG. 3. The scaling functions continue to satisfy

$$f(\bar{n}, 0) = 0, \quad (3.9)$$

and

$$f'(\bar{n}, 0) > 0, \quad (3.10)$$

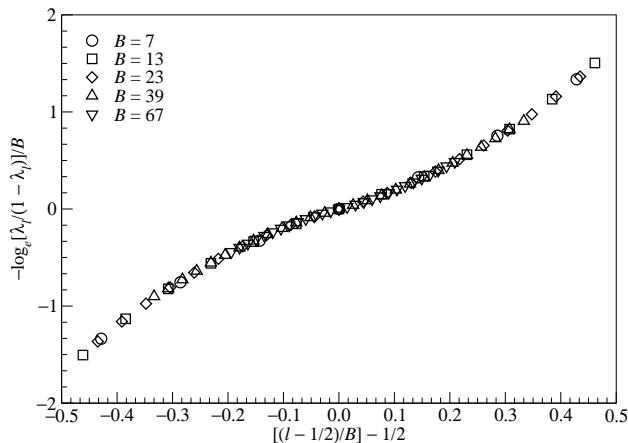


FIG. 2: Plot of  $-B^{-1} \log_e[\lambda_l/(1-\lambda_l)]$  as a function of the scaling variable  $x \equiv [(l - \frac{1}{2})/B] - 1/2$  for various block sizes at half-filling, showing a scaling collapse onto the scaling function  $f(x)$ . For  $B > 23$ , the largest and smallest pseudo-energies are severely affected by numerical truncation errors in the diagonalization routines, and thus not shown.

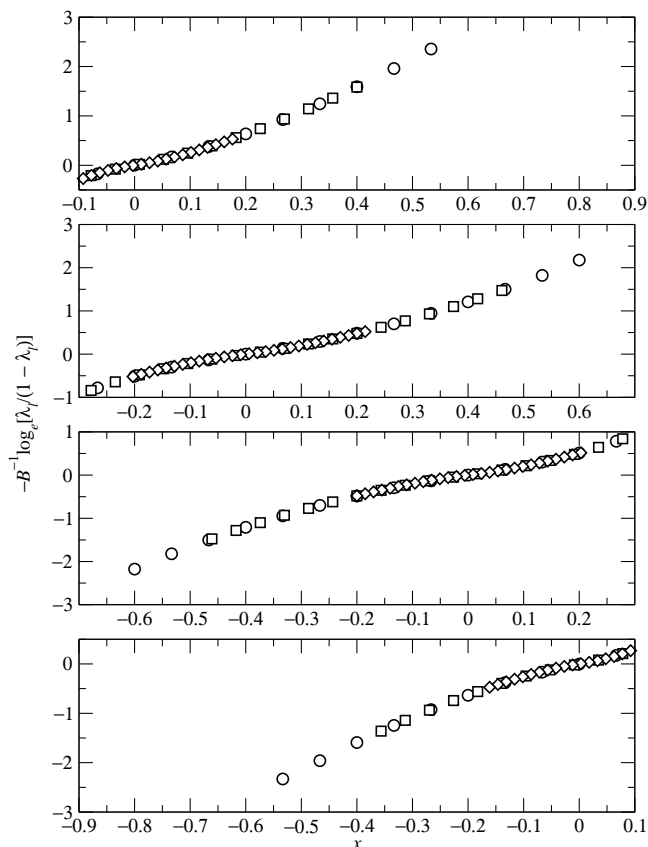


FIG. 3: Scaling collapses for (from top to bottom)  $\bar{n} = 0.1, 0.3, 0.7$  and  $0.9$ , plotted against the scaling variable  $x \equiv [(l - \frac{1}{2})/B] - \bar{n}$ , for three different block sizes:  $B = 15$  ( $\circ$ ),  $B = 23$  ( $\square$ ) and  $B = 67$  ( $\diamond$ ).

but  $f(\bar{n}, x)$  is no longer an odd function of  $x$  for  $\bar{n} \neq \frac{1}{2}$ . Instead, the particle-hole symmetry inherent in our model is manifested as

$$f(\bar{n}, -x) = -f(1 - \bar{n}, x). \quad (3.11)$$

From (2.8) and (3.6), we can write  $\lambda_l$  as

$$\lambda_l = \frac{1}{\exp(Bf) + 1}, \quad (3.12)$$

which tells us that  $f(\bar{n}, x)$  plays the role of a dispersion relation  $\epsilon(k)$ , while  $B$  plays the role of the inverse temperature  $\beta$ . This confirms our suspicion that the effect of cutting a block out of an overall system in its ground state at  $T = 0$  is to ascribe to the block an effective temperature. As expected, this effective temperature approaches zero as the block size is increased, since we are keeping more and more information about the overall system, which we know to be at  $T = 0$ .

## B. Normalization Constant

Having understood that  $\lambda_l$  is related to the scaling function  $f(\bar{n}, x)$  as in (3.12), we are now ready to investigate the scaling behaviour of the normalization constant  $\mathcal{Q}^{-1}$ , which is related to  $\lambda_l$  by (2.9). We do this first at half-filling. As can be seen from FIG. 1, at half-filling roughly half of the  $\lambda_l$  are approximately one, whereas the other half are approximately zero. The product  $\prod_l (1 - \lambda_l)$  is therefore determined primarily by the  $\sim B/2$   $\lambda_l$ 's that are nearly one. For these eigenvalues,  $\exp[Bf(x)] \ll 1$  and thus  $1 - \lambda_l \approx \exp[Bf(x)]$  (when it is clear what the filling fraction is, we will drop the argument  $\bar{n}$  in  $f(\bar{n}, x)$  to keep the notations neat). With this, we find that

$$\begin{aligned} \mathcal{Q}^{-1} &= \prod_{l=1}^B (1 - \lambda_l) \approx \prod_{l=1}^{B/2} \exp[Bf(x)] \\ &\approx \exp \left\{ B \int_{-1/2}^0 f(x) dx \right\} \\ &= \exp \left\{ -B \int_0^{1/2} f(x) dx \right\}, \end{aligned} \quad (3.13)$$

where we made use of the observed odd symmetry of the scaling function in (3.4) when the overall system is at half-filling, so that the integral within the exponent is positive. From (3.13), we see that  $\mathcal{Q}^{-1}$  decreases exponentially with block size  $B$ .

In general, for  $\bar{n}$  not too close to zero, where the argument that those  $\lambda_l$ 's that are near one makes the dominant contribution holds, we find that

$$\begin{aligned} \mathcal{Q}^{-1} &\approx \exp \left\{ B \int_{-\bar{n}}^0 f(\bar{n}, x) dx \right\} \\ &= \exp \left\{ -B \int_0^{\bar{n}} f(1 - \bar{n}, x) dx \right\}, \end{aligned} \quad (3.14)$$

where we made use of (3.11). For  $\bar{n}$  very close to zero, there are a handful of  $\lambda_l$ 's of  $O(1)$ , and the rest are all nearly zero, behaving like  $\lambda_l \approx \exp[-Bf(\bar{n}, x)]$ . Ignoring these handful of  $O(1)$   $\lambda_l$ 's, we find that the contribution to  $\mathcal{Q}^{-1}$  from those  $\lambda_l \ll 1$  is proportional to the product  $\prod_l(1 - \lambda_l) \approx 1 - \sum_l \lambda_l$ , and so

$$\mathcal{Q}^{-1} \propto \left[ 1 - \int_0^{1-\bar{n}} e^{-Bf(\bar{n}, x)} dx \right]. \quad (3.15)$$

The integral can be evaluated as a cumulant expansion, but we can already see that for large  $B$ , the integral will not be important, and thus  $\mathcal{Q}^{-1}$  derives most of its value from the few  $O(1)$   $\lambda_l$ 's. In contrast, when  $\bar{n}$  is very close to 1, then most of the eigenvalues  $\lambda_l$  of  $G$  are close to 1, and these continue to dominate the product  $\prod_l(1 - \lambda_l)$ , and the asymptotic formula derived in (3.13) continues to be valid.

#### IV. DENSITY MATRIX WEIGHTS: IMPLICATIONS OF EIGENVALUE SCALING

With our understanding of the structure of the many-particle density matrix eigenvalues and eigenstates developed in Section II A, and on the scaling behaviour of the single-particle found in Section III, we want to now address the question of how much of the Hilbert space we can truncate. Clearly, the answer to this question depends on what measure of error we intend to use as our criteria for judging how well the truncated Hilbert space describes the physics associated with the parent model. In this section we look at the most common measure of error, used in the DMRG<sup>1,2</sup> and quantum chemistry calculations:<sup>10-12</sup> for a properly normalized density matrix, the density matrix weights  $w_L$  satisfy the sum rule

$$\sum_L w_L = 1. \quad (4.1)$$

If the ordinal numbers  $L$  are chosen such that  $w_L$  is ranked in decreasing order, and a total of  $L_{\max}$  density matrix eigenstates are retained, then the truncated weight

$$W_t = \sum_{L \leq L_{\max}} w_L \leq 1, \quad (4.2)$$

and the discarded weight

$$\epsilon = 1 - W_t \quad (4.3)$$

are frequently used as figures of merit for the truncation scheme, since for a bounded operator  $A$ , the truncation error in  $\langle A \rangle$  is  $O(\epsilon)$ .

#### A. The Gapless Chain of Noninteracting Spinless Fermions

Instead of diving in to look at  $W_t$  or  $\epsilon$ , let us consider first a related question: how large is the maximum weight for a block of  $B$  sites embedded within an overall system of gapless noninteracting spinless fermions? For our discussions, we will consider the half-filled case; it will be straightforward to extend the arguments presented below to  $\bar{n} \neq \frac{1}{2}$ . For convenience, let us take  $B$  to be even.<sup>19</sup> Let us denote by  $|F\rangle$ , where  $F = B/2$ , the many-particle density matrix eigenstate having the largest weight. This state is always kept in the operator-based truncation scheme. Recall from Section II that, as shown in FIG. 4(b), this is the analog among density matrix eigenstates of the Fermi sea ground state among energy eigenstates. In this  $B/2$ -particle state, the single-particle pseudo-energy is filled up to just before  $x = 0$ , which we shall call the *pseudo-Fermi level*. The many-

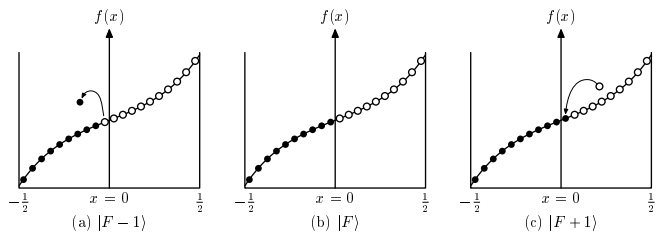


FIG. 4: Schematic diagram showing the three many-particle density matrix eigenstates, (a)  $|F-1\rangle$ , (b)  $|F\rangle$  and (c)  $|F+1\rangle$ , with the largest weights, for a block of  $B$  ( $B$  even) sites within a overall system that is half-filled.

particle density matrix eigenstates of the block, of which there are two, having the next largest weights will be called  $|F-1\rangle$  (FIG. 4(a)) and  $|F+1\rangle$  (FIG. 4(c)), having respectively one less or one more particle.

We can understand the weight ratio  $w_{F-1}/w_F$  or  $w_{F+1}/w_F$  as follows. By (2.2),  $|F\rangle$  is the state with  $n_l = 1$  for  $l = 1, \dots, B/2$  and  $n_l = 0$  for  $l = B/2 + 1, \dots, B$ . The state  $|F+1\rangle$  differs only in having  $n_{B/2+1} = 1$ , while  $|F-1\rangle$  differs only in having  $n_{B/2} = 0$ . Near the pseudo-Fermi level, the scaling function has a slope of  $f'(0)$ , while the spacing between adjacent pseudo-energies on the rescaled  $l/B$  axis is  $1/B$ . Thus  $\varphi_{B/2+1} - \varphi_{B/2} \approx f'(0)$ . But when the actual filling is  $\bar{n} = \frac{1}{2}$ , we know by particle-hole symmetry that  $\varphi_{B/2+1} = -\varphi_{B/2}$ , so  $\varphi_{B/2} \approx -f'(0)/2$  and  $\varphi_{B/2+1} \approx f'(0)/2$ . It follows from (2.2), that

$$\frac{w_{F+1}}{w_F} = \frac{w_{F-1}}{w_F} \approx \exp(-f'(0)). \quad (4.4)$$

For  $\bar{n} \neq \frac{1}{2}$ , (3.6) would tell us that these ratios are approximately  $\exp(-f'(\bar{n}, 0))$ .

This is quite different from what would happen when the 'block' contains half of the entire system, as considered in the standard DMRG algorithm, or in Ref.8.

If the fraction  $(B/N)$  in the block approached one, the state  $|F\rangle$  must become the Fermi sea ground state of the overall system, and consequently contains all the weight. If the block is merely a finite fraction of the system, we still expect a much larger ratio than (4.4). It would be interesting to check the behaviour of the ratios in (4.4) for the case  $B, N \rightarrow \infty$  with  $B/N = 1/2$ , but we have not investigated this.

### B. The Gapped Chain of Noninteracting Spinless Fermions

For the purpose of understanding the pseudo-energy spectrum of non-interacting systems better, we also considered the dimerized tight-binding Hamiltonian

$$H = -t \sum_{j=1}^N [1 + (-1)^j \delta] (c_j^\dagger c_{j+1} + c_{j+1}^\dagger c_j), \quad (4.5)$$

where the hopping integral  $t$  is modulated by the  $(-1)^j \delta$  term to produce an energy gap. Henceforth we choose the scale of energy to be such that  $t = 1$ . This system was solved analytically by Gebhard *et al.*<sup>16</sup> wherein the Hamiltonian can be written as

$$H = \sum_{|k| < \frac{\pi}{2a}} E(k) (a_{k,+}^\dagger a_{k,+} - a_{k,-}^\dagger a_{k,-}), \quad (4.6)$$

with  $E(k) = \sqrt{\epsilon^2(k) + \Delta^2(k)}$ , where  $\epsilon(k) = -2 \cos k$  and  $\Delta(k) = 2\delta \sin k$ . In terms of  $\Delta(k)$  and  $\epsilon(k)$ , we can define an angle  $\phi_k$  such that  $\tan 2\phi_k = \Delta(k)/\epsilon(k)$ , and whose sine and cosine we denote as  $\alpha_k = \cos \phi_k$ ,  $\beta_k = \sin \phi_k$ . In terms of these, the operators  $a_{k,+}$  and  $a_{k,-}$  for the upper and lower bands respectively are given by

$$\begin{aligned} a_{k,-} &= \alpha_k \tilde{c}_k + i \beta_k \tilde{c}_{k+\pi}, \\ a_{k,+} &= -\beta_k \tilde{c}_k + i \alpha_k \tilde{c}_{k+\pi}. \end{aligned} \quad (4.7)$$

At half-filling, the lower band is completely filled while the upper band is completely empty, and the ground state can be written simply as

$$|\Psi\rangle = \prod_{|k| < \frac{\pi}{2}} a_{k,-}^\dagger |0\rangle. \quad (4.8)$$

For this ground state, the two-point function is given by

$$G_{ij} = \frac{1}{2\pi} \int_{-\frac{\pi}{2}}^{\frac{\pi}{2}} dk e^{ik(i-j)} \frac{\cos k - i(-1)^i \delta \sin k}{\sqrt{\cos^2 k + \delta^2 \sin^2 k}}, \quad (4.9)$$

using which we can construct the block Green function matrix  $G$ , and hence using (2.7) the pseudoenergies which correspond to the density matrix eigenvalues. For a fixed block size of  $B = 23$ , the pseudo-energy spectra for different hopping modulation  $\delta$  is shown in FIG. 5, compared to that of the gapless case. Scaling behaviour of the

single-particle pseudo-energies was found for all  $\delta$ , each governed by a different scaling function  $f(\bar{n}, \delta, x)$ . The scaling collapse plot for  $\delta = 0.5$  is shown in FIG. 6, compared to the scaling function  $f(\bar{n}, \delta = 0, x)$  for the gapless case.

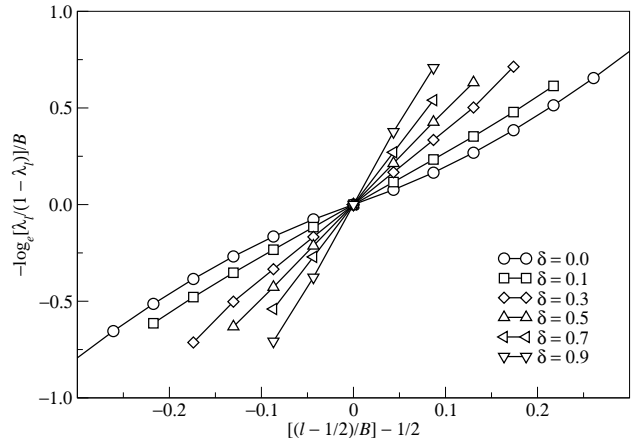


FIG. 5: Plot of  $-B^{-1} \log_e [\lambda_i / (1 - \lambda_i)]$  as a function of the scaling variable  $x = (l - \frac{1}{2})/B - \frac{1}{2}$ , for a block of size  $B = 23$ , with different hopping modulations  $\delta = 0.1, 0.3, 0.5, 0.7, 0.9$ . Pseudo-energies for  $|x| > 0.2$  for  $\delta > 0$  are not shown because these are severely affected by numerical errors incurred in the numerical integration and diagonalization routines. The various sets of straight line segments are intended to guide the eye in visualizing the data.

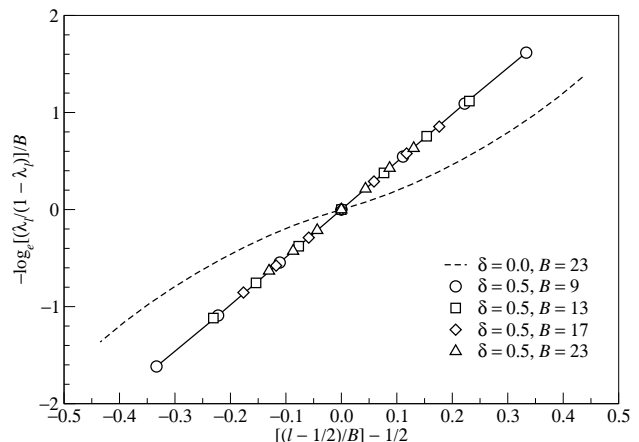


FIG. 6: Plot of  $-B^{-1} \log_e [\lambda_i / (1 - \lambda_i)]$  as a function of the scaling variable  $x = (l - \frac{1}{2})/B - \frac{1}{2}$ , for hopping modulation  $\delta = 0.5$  and different block sizes  $B = 9, 13, 17, 23$ . The pseudo-energies for  $|x| > 0.3$  are not shown as these are severely affected by numerical errors in the numerical integration and diagonalization routines. Also shown, is an approximate dashed curve for the scaling function  $f(x)$  for  $\bar{n} = \frac{1}{2}$  and  $\delta = 0$ , obtained from the data for  $B = 23$ . The straight line segments are intended to guide the eye in visualizing the data.

Repeating our analysis for the three density matrix eigenstates with the largest weights, we find again



that the ratios of density matrix weights  $w_{F+1}/w_F$  and  $w_{F-1}/w_F$  to be independent of block size  $B$  when the overall system is at half-filling. However, these ratios depend strongly on the hopping modulation  $\delta$ . As we can see from FIG. 5, the slope of the scaling curve at  $x = 0$  is steeper for larger  $\delta$ . This indicates that — everything else being equal for finite  $B$  — a smaller fraction of density matrix states is needed to capture the same total weight if the system is gapped.

We have not investigated the case  $B/N \rightarrow 1/2$ , as in the standard DMRG algorithm, but we naturally expect the ratio to increase in a gapped system. Thus  $|F\rangle$  would be a better approximation to the ground state in a gapped system than in a gapless system, which is known as an empirical fact in the DMRG context. Our approach, if extended to the case  $B/N > 0$ , would give an analytic justification for this common observation.

### C. Largest Density Matrix Weight

For even  $B$  blocks on a gapless chain of noninteracting spinless fermions described the Hamiltonian (1.1), the largest density matrix weight  $w_F$  can be numerically computed reliably till  $B \approx 20$ , and its dependence on  $B$  is shown in FIG. 7. Also shown in FIG. 7 is a fit of the numerical data to

$$w_F(B) = w_{F,\infty} + \Delta w_F \exp(-B/B_0), \quad (4.10)$$

where  $w_{F,\infty}$ ,  $\Delta w_F$  and  $B_0$  are curve-fitting parameters. Here the exponentially decaying term is merely chosen to produce a good curve fit — we believe the  $B$ -dependence may be more complex — but what is interesting is the fact that  $w_F$  tends to a constant,  $w_{F,\infty}$ , in the limit of  $B \rightarrow \infty$ . We find that we can understand this in terms of the scaling formulas developed so far.

From Section II we saw that the largest many-particle density matrix weight  $w_F$  corresponds to the situation for which all PELs below the pseudo-Fermi level  $\varphi_F = 0$  are occupied, and all those above are empty. This means that

$$w_F = \mathcal{Q}^{-1} \prod_{l < l_F} e^{-\varphi_l}. \quad (4.11)$$

Using the fact that  $\mathcal{Q}$  can be written explicitly as

$$\mathcal{Q} = \prod_l (1 + e^{-\varphi_l}), \quad (4.12)$$

we then find that

$$w_F = \prod_{l < l_F} \frac{e^{-\varphi_l}}{1 + e^{-\varphi_l}} \prod_{l > l_F} \frac{1}{1 + e^{-\varphi_l}} = \prod_l \frac{1}{1 + e^{-|\varphi_l|}}. \quad (4.13)$$

To evaluate  $w_F$ , we evaluate first its logarithm, which is

$$-\log_e w_F = \sum_l \log_e (1 + e^{-|\varphi_l|}). \quad (4.14)$$

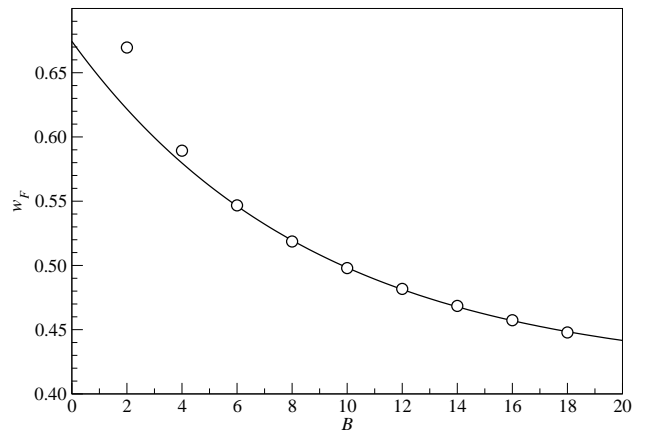


FIG. 7: Plot of the largest density matrix weight  $w_F$  as a function of the block size  $B$  for  $B$  even. The solid curve shown is a fit of the form  $w_F = w_{F,\infty} + \Delta w_F \exp(-B/B_0)$ . The best fit to this small data set is obtained by neglecting the data points for  $B = 2$  and  $B = 4$ , for which we get  $w_{F,\infty} = 0.41$ ,  $\Delta w_F = 0.26$  and  $B_0 = 0.11$ .

Here we make two approximations. Firstly, because of (3.6), we know that  $\varphi_l \propto B$ , and so except for a handful of single-particle pseudo-energies  $\varphi_l$  very near  $\varphi_F$ , all the exponentials are very small numbers. Using the approximation  $\log_e(1 + x) \approx x$  for  $x \ll 1$ , we write (4.14) as

$$-\log_e w_F \approx \sum_l e^{-|\varphi_l|}. \quad (4.15)$$

Secondly, we note that because of (3.6), single-particle pseudo-energies far away from  $\varphi_F = 0$  will contribute negligibly to the above sum. For  $B$  sufficiently large, those single-particle pseudo-energies making significant contribution in (4.14) will lie within a small interval about  $l_F$  where a linear approximation of the form

$$\varphi_l \approx B f'(0) \frac{l - l_F}{B} = f'(0)(l - l_F) \quad (4.16)$$

adequately describes the pseudo-dispersion relation. Substituting (4.16) into (4.15), we find then that

$$\begin{aligned} -\log_e w_F &\approx \sum_{l=1}^B e^{-f'(0)|l-l_F|} \\ &\approx 2 \sum_{l > l_F} e^{-f'(0)(l-l_F)}. \end{aligned} \quad (4.17)$$

This is a geometric series which we can readily sum to give

$$-\log_e w_F = \frac{2}{1 - \exp(-f'(0))}, \quad (4.18)$$

i.e. the largest density matrix weight  $w_F$  is found to approach a constant value of

$$w_F = \exp \left[ -\frac{2}{1 - \exp(-f'(0))} \right] \quad (4.19)$$

as  $B \rightarrow \infty$ . From FIG. 2 and FIG. 3, we see that  $f'(0) \approx 5$ , and so this asymptotic value of  $w_F$  is approximately 0.13. This is smaller than the  $w_{F,\infty} = 0.41$  found numerically.

#### D. Discarded Weight

Now that we understand more about the scaling behaviour of the largest density matrix weight  $w_F$ , let us analyze the discarded weight incurred by the operator-based DM truncation scheme. We compute numerically the discarded weight incurred by the operator-based DM truncation scheme and that incurred by the weight-ranked DM truncation scheme, and show them in FIG. 8 as a function of the number of many-body states kept as a comparison. As we can see, the discarded weight incurred by the operator-based DM truncation scheme is larger compared to the weight-ranked DM truncation scheme, for the same number of many-particle eigenstates kept. This is expected, since the weight-ranked DM truncation scheme is by definition the most efficient scheme in exhausting the sum rule given in (4.1). In spite of this seemingly poorer ‘convergence’ property, we believe that the operator-based truncation scheme has advantages that cannot be reproduced by the weight-ranked truncation scheme, to be argued in detail in Section VI.

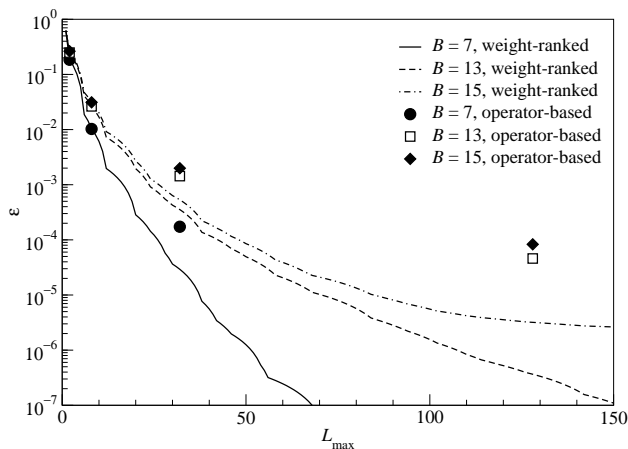


FIG. 8: Discarded weight  $\epsilon$  as a function of the number of states kept: weight-ranked (as done in the DMRG), and operator-based.

Writing the total density matrix weight explicitly as

$$W = \mathcal{Q}^{-1} \prod_{\text{kept}} (1 + e^{-\varphi_l}) \prod_{\text{below}} (1 + e^{-\varphi_l}) \prod_{\text{above}} (1 + e^{-\varphi_l}), \quad (4.20)$$

where the subscript ‘kept’, ‘below’ and ‘above’ refer to PELs retained, approximated as always occupied and approximated as always empty in the operator-based truncation scheme respectively. The truncated weight  $W_t$  cal-

culated from the operator-based truncation scheme is

$$W_t = \mathcal{Q}^{-1} \prod_{\text{kept}} (1 + e^{-\varphi_l}) \prod_{\text{below}} e^{-\varphi_l} \prod_{\text{above}} 1. \quad (4.21)$$

Since  $W = 1$ , the ratio  $W_t/W = W_t$  can be written as

$$\begin{aligned} W_t &= \prod_{\text{below}} \frac{e^{-\varphi_l}}{1 + e^{-\varphi_l}} \prod_{\text{above}} \frac{1}{1 + e^{-\varphi_l}} \\ &= \prod_{\text{below}} \frac{1}{1 + e^{\varphi_l}} \prod_{\text{above}} \frac{1}{1 + e^{-\varphi_l}}. \end{aligned} \quad (4.22)$$

This expression has a simple interpretation in terms of the pseudo-occupation numbers  $\{\lambda_l\}$ . Using (2.8), we find that we can write  $W_t$  as

$$W_t = \prod_{\text{below}} \lambda_l \prod_{\text{above}} (1 - \lambda_l), \quad (4.23)$$

i.e. the truncated weight  $W_t$  is given by the product of pseudo-occupation numbers  $\lambda_l$  of those PELs we insist are always occupied, together with the product of the single-hole pseudo-occupation numbers  $(1 - \lambda_l)$  of those PELs we insist are always empty. From FIG. 1 we see that  $\lambda_l$  changes fairly rapidly from  $\lambda_l \lesssim 1$  to  $\lambda_l \gtrsim 0$ , over a small range of PELs. Therefore, it appears that there is a fairly large range of  $l$ 's for which  $\lambda_l$  is very close to one or very close to zero. However, this does not mean that we should perform an operator-based truncation scheme keeping only the small number of PELs whose  $\lambda_l$ 's are significantly different from one or zero. This is because  $W_t$  is bounded from above by

$$W_t \leq \prod_{\text{below}} \lambda_{\max} \prod_{\text{above}} (1 - \lambda_{\min}) \leq (\lambda^*)^{(1-\gamma)B}, \quad (4.24)$$

where  $\gamma$  is the fraction of PELs retained in the operator-based truncation scheme, and

$$\lambda^* = \max(\lambda_{\max}, 1 - \lambda_{\min}). \quad (4.25)$$

Because the exponent is  $O(B)$ , this number can still be very small.

This brings us to the question we posed in the beginning of this section: how much of the Hilbert space do we truncate? If  $W_t$  is the only criterion then we see that a compromise is necessary. For a small block, the number of PELs with  $\lambda_l$  significantly different from one or zero is a sizeable fraction of the total number of PELs, but this number is manageable. For a large block, the number of PELs with  $\lambda_l$  significantly different from one or zero is a tiny fraction of the total number of PELs, but we still need  $\gamma$  to be reasonably large for  $W_t$  to be appreciable in magnitude. This of course means that an unmanageably large number of PELs has to be retained.

To make the above discussions more water-tight, let us make use of the scaling relations obtained thus far to find a formula relating the truncated weight  $W_t$  to both

the block size  $B$  and the fraction  $\gamma$  of PELs retained. Taking the logarithm of (4.22) we find, using the fact that  $\exp(-|\varphi_l|) \ll 1$  for  $l$  far below  $l_F$ , and  $\exp(-\varphi_l) \ll 1$  for  $l$  far above  $l_F$ , that

$$\begin{aligned}
-\log_e W_t &= \sum_{\text{below}} \log_e(1 + e^{\varphi_l}) + \sum_{\text{above}} \log_e(1 + e^{-\varphi_l}) \\
&\approx \sum_{\text{below}} e^{\varphi_l} + \sum_{\text{above}} e^{-\varphi_l} \\
&= \sum_{l < l_F} e^{\varphi_l} - \sum_{l=l_F-\gamma B/2}^{l_F} e^{\varphi_l} + \\
&\quad \sum_{l > l_F} e^{-\varphi_l} - \sum_{l_F}^{l_F+\gamma B/2} e^{-\varphi_l} \\
&= \Phi^* - \sum_{l=l_F-\gamma B/2}^{l_F} e^{\varphi_l} - \\
&\quad \sum_{l_F}^{l_F+\gamma B/2} e^{-\varphi_l},
\end{aligned} \tag{4.26}$$

where  $\Phi^*$  is a constant.

If  $B$  is large and  $\gamma$  small, then the linear approximation (4.16) for  $\varphi_l$  is valid, in which case the two sums in (4.26) are equal, and given by

$$\begin{aligned}
\sum_{l_F}^{l_F+\gamma B/2} e^{-\varphi_l} &\approx \sum_{l_F}^{l_F+\gamma B/2} e^{-f'(0)(l-l_F)} \\
&= \frac{1 - \exp(-\gamma B f'(0)/2)}{1 - \exp(-f'(0))}.
\end{aligned} \tag{4.27}$$

With this, we can write  $W_t$  as

$$W_t \approx W^* \exp \left[ \frac{2}{1 - e^{-f'(0)}} \left( 1 - e^{-\gamma B f'(0)/2} \right) \right], \tag{4.28}$$

where  $W^* = \exp(-\Phi^*)$ . We can find  $W^*$  by taking the limit  $\gamma \rightarrow 0$ , in which case we retain no degree of freedom in the PELs. Within the operator-based truncation scheme, this means that we insist all PELs below  $\varphi_F$  to be always occupied and all those above  $\varphi_F$  to be always empty, i.e. only the density matrix eigenstate with the largest weight is retained, and we should have

$$W_t = w_F = W^*, \tag{4.29}$$

and so

$$W_t \approx w_F \exp \left[ \frac{2}{1 - e^{-f'(0)}} \left( 1 - e^{-\gamma B f'(0)/2} \right) \right]. \tag{4.30}$$

This can be simplified further, using (4.19) to get

$$W_t \approx \exp \left[ -\frac{2}{1 - e^{-f'(0)}} e^{-\gamma B f'(0)/2} \right]. \tag{4.31}$$

In the limit of  $\gamma \rightarrow 1$ , we see from the above expression that  $W_t$  does not tend to one, but we understand that this is because the linear approximation (4.16) is only valid for a small range of PELs about  $\varphi_F$ , i.e. only for small  $\gamma$ . In this regime, we may further approximate  $W_t$  as

$$\begin{aligned}
W_t &\approx \exp \left[ -\frac{2}{1 - e^{-f'(0)}} \left( 1 - \frac{f'(0)\gamma B}{2} \right) \right] \\
&\approx w_F \exp \left( \frac{f'(0)}{1 - e^{-f'(0)}} l_{\max} \right),
\end{aligned} \tag{4.32}$$

where

$$l_{\max} = \gamma B \tag{4.33}$$

is the number of PELs retained. As we can see, for small  $\gamma$ , the truncated weight  $W_t$  increases exponentially with  $l_{\max}$ . Also, whenever (4.32) is valid, we get approximately the same truncated weight  $W_t$  whether we use  $B = 100$  and  $\gamma = 0.2$  or  $B = 200$  and  $\gamma = 0.1$ . We will see in Section VI that whenever the retained  $\gamma B$  PELs lies within the regime where the pseudo-dispersion relation is linear, the truncation errors are essentially determined by  $l_{\max} = \gamma B$ .

## V. SINGLE-PARTICLE DENSITY MATRIX EIGENFUNCTIONS

### A. *A Priori* Expectations

As noted already in Section IIC, in the many-body eigenstates with largest weights, all the very negative PELs will be occupied and all the very positive PELs will be empty. The only PELs with significant varying occupancy are those near the pseudo-Fermi level.

By construction, the many-body density matrix eigenstates with large weights constitute the likely configurations of the block. The difference between the large-weight eigenstates of the  $P$ -particle and  $(P+1)$ -particle sectors of the density matrix is in the application of a creation operator  $f_l^\dagger$  such that the pseudo-energy  $|\varphi_l|$  is close to  $\varphi_F = 0$ . In real space, it is likeliest that we can add a particle near the ends of the  $B$ -site block, for one can imagine that, in the first configuration, this particle was just past the end in an adjacent block, and we merely hopped it a short distance across the boundary to create the state of  $(P+1)$  particles on the block in question. It follows that the single-particle eigenfunctions with single-particle pseudo-energies near the pseudo-Fermi level have their greatest amplitude near the block's boundaries. In other words, it is the sites near the end that are most correlated with the environmental information that we discarded.

## B. General Features

As noted earlier, the eigenstates of  $\rho_B$  are all built up from the eigenstates  $|\chi_l\rangle$  of  $G$ , which are simultaneously the one-particle eigenstates of  $\rho_B$ . As such, the effects of basis truncation, particularly in obtaining a truncated expansion of the target state  $|\Psi\rangle$ , must be understood in terms of the features of these one-particle eigenstates. The real-space features of  $|\chi_l\rangle$  can most easily be understood in terms of the corresponding eigenfunctions  $\chi_l(j)$ , where  $j = 1, \dots, B$  are sites on the block. At half-filling, the probability densities  $|\chi_l(j)|^2$  exhibit particle-hole symmetry, as is shown in FIG. 9 for the example of  $B = 9$ . In general, by node counting, we see that the sequence of  $B$  single-particle eigenfunctions are in one-to-one correspondence with the sequence of  $B$  plane wave states on the block, where the ordinal number  $l$  of the single-particle eigenfunctions is related to the wavevector  $k$  of the plane wave states on the block by

$$k = \frac{2\pi(l-1)}{Ba}, \quad l = 1, \dots, B. \quad (5.1)$$

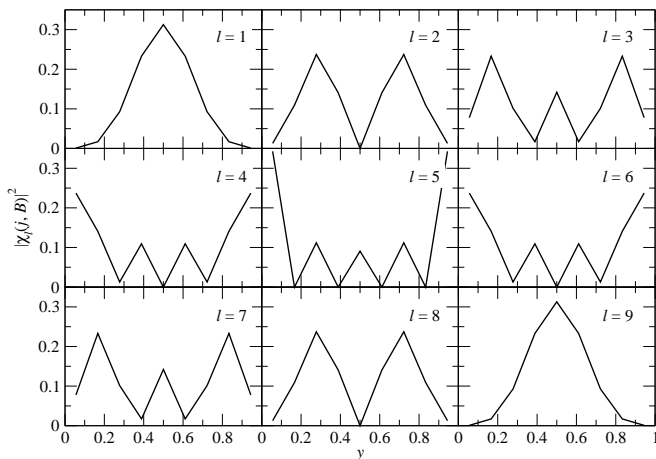


FIG. 9: Probability density of the normalized one-particle eigenfunctions  $\chi_l(j)$  (plotted against the scaling variable  $y = (j - \frac{1}{2})/B$ ) of  $\rho_B$  on a block of  $B = 9$  sites at half-filling, showing the particle-hole symmetry of the overall system. The subplots are arranged in order of increasing pseudo-energy.

## C. Scaling Behaviour

For odd  $B$ , the pseudo-energy  $\varphi_{(B+1)/2}$  sits at the pseudo-Fermi level, and we may call the corresponding eigenfunction  $\chi_F(j) \equiv \chi_{(B+1)/2}(j)$  the *pseudo-Fermi eigenfunction*. The probability density associated with  $\chi_F(j)$  has nodes at every even  $j$ , as shown in in FIG. 10 for the case of  $B = 23$ . The most prominent feature of the pseudo-Fermi eigenfunction, i.e. the amplitude being strongest near the boundaries of the block, was first

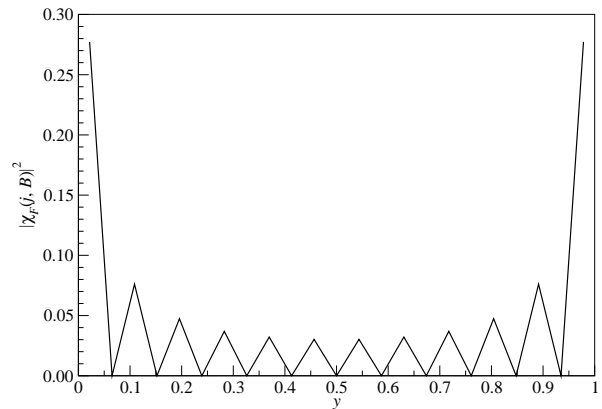


FIG. 10: Probability density function  $|\chi_F(j, B)|^2$  of the pseudo-Fermi eigenfunction for  $B = 23$ , plotted against the scaled variable  $(j - \frac{1}{2})/B$ .

observed by White.<sup>2</sup> This appears to be a generic feature that occurs in both integrable and nonintegrable 1-dimensional systems. Using the example of a chain of coupled harmonic oscillators, Gaiete explained this “concentration of resolution of quantum states near the boundaries” as a simple consequence of angular quantization of the density matrix.<sup>17</sup>

To analyze  $|\chi_F(j, B)|^2$  (where we write the  $B$  dependence of  $\chi_F(j)$  more explicitly) more carefully, we first rescale the eigenvectors obtained from Octave<sup>18</sup> such that

$$|\chi_F((B+1)/2, B)|^2 = 1 \quad (5.2)$$

for  $B = 4p + 1$ ,  $p = 1, 2, \dots$ . For  $B = 4p + 3$ ,  $|\chi_F((B+1)/2, B)|^2 = 0$  and the rescaling cannot be carried out as unambiguously as for the  $B = 4p + 1$  series. This rescaling is harmless, since eigenvectors are only defined up to an arbitrary normalization. After this trivial rescaling, we find that the pseudo-Fermi probability density can be put in a scaling form

$$|\chi_F(j, B)|^2 \cong N(B)g(y) \frac{\frac{1}{2}[1 - (-1)^j]}{\sin^2 \pi y}, \quad (5.3)$$

where  $y \equiv (j - \frac{1}{2})/B$  and  $g(y)$  is the scaling function shown in FIG. 11.

In (5.3),  $N(B)$  is a  $B$ -dependent normalization factor, chosen to ensure that the pseudo-Fermi wavefunction given is properly normalized in the limit of  $B \rightarrow \infty$ , i.e.

$$\lim_{B \rightarrow \infty} \sum_{j=1}^B |\chi_F(j, B)|^2 = 1. \quad (5.4)$$

Although we cannot compute  $N(B)$  analytically, we venture a guess to its  $B$ -dependence by noting that the functions  $g(y)$  and  $\sin \pi y$  are not very different from the func-

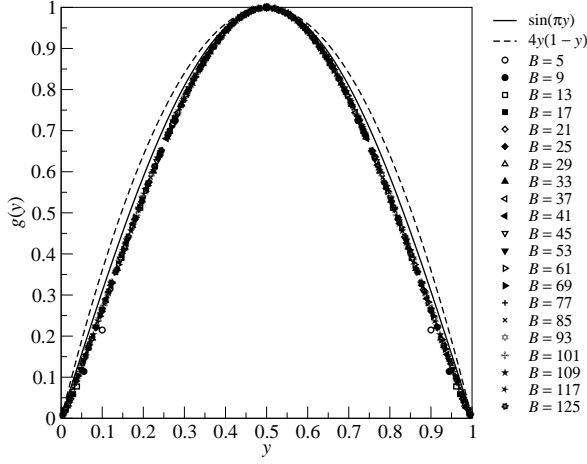


FIG. 11: Plot of the rescaled envelope function  $g(y)$  for various block sizes  $B = 4p + 1$ ,  $p = 1, 2, \dots$ , compared against  $\sin \pi y$  and  $4y(1 - y)$ , where  $y = (j - \frac{1}{2})/B$  is the rescaled coordinate on the block.

tion  $4y(1 - y)$ , and so we expect

$$\begin{aligned} & \sum_{j=1}^B g(y) \frac{\frac{1}{2}[1 - (-1)^j]}{\sin^2 \pi y} \\ & \sim \sum_{j=1}^B 4y(1 - y) \frac{\frac{1}{2}[1 - (-1)^j]}{[4y(1 - y)]^2} \\ & = \frac{1}{4} \sum_{j \text{ odd}}^B \left[ \frac{1}{y} + \frac{1}{1 - y} \right], \end{aligned} \quad (5.5)$$

which we can easily work out to have the form

$$\sum_{j=1}^B g(y) \frac{\frac{1}{2}[1 - (-1)^j]}{\sin^2 \pi y} \sim B (\log_e B + C), \quad (5.6)$$

where  $C$  is a constant. Numerically, the best fit for  $N(B)$  in the range of block sizes  $B = 33$  to  $B = 125$  is obtained with

$$N^{-1}(B) = 0.249B \log_e B + 0.668B. \quad (5.7)$$

Because of the enhanced amplitude near the edge of the block exhibited in the real-space structure of density matrix eigenfunctions with single-particle pseudo-energies close to the pseudo-Fermi level, and conversely, enhanced amplitude near the center of the block exhibited in the real-space structure of density matrix eigenfunctions with single-particle pseudo-energies far away from the pseudo-Fermi level, we worry that these eigenfunctions might not be a good basis to use for expanding spatially uniform plane waves, which are the true single-particle energy eigenstates in our model. We address this concern in Section VI C.

## VI. OPERATOR-BASED DENSITY MATRIX TRUNCATION APPLIED TO DISPERSION RELATION

In a gapless system, we conjecture that low-lying excitations *above* the ground state are built from the same operators as the long-wavelength fluctuations *within* the ground state. This supposition is certainly validated if the system has a continuous symmetry and the long-wavelength modes are Goldstone modes. In general it is justified by the relationships between correlation functions (for the ground-state fluctuations) and response functions (for low-energy excitations).

Despite its poor convergence properties as far as exhausting the sum rule (4.1) is concerned, the operator-based truncation would still get the salient features of the physics right. We check this by projecting the Hamiltonian in (1.1) onto the truncated set of fermion operators  $f_l$ , and calculate the dispersion relation therefrom. There are two physical quantities of interest here: (a) for odd number of sites  $B$ , the middle band crosses the Fermi level, and we can ask how the Fermi velocity, given by the slope of the dispersion relation at the Fermi level, scales with  $B$  and the fraction  $\gamma$  of fermion operators kept; or (b) for even  $B$ , a band gap develops as a result of truncation at the Fermi level, and we can ask how the size of this band gap depends on  $B$  and  $\gamma$ .

### A. Energy Gap at Fermi Level

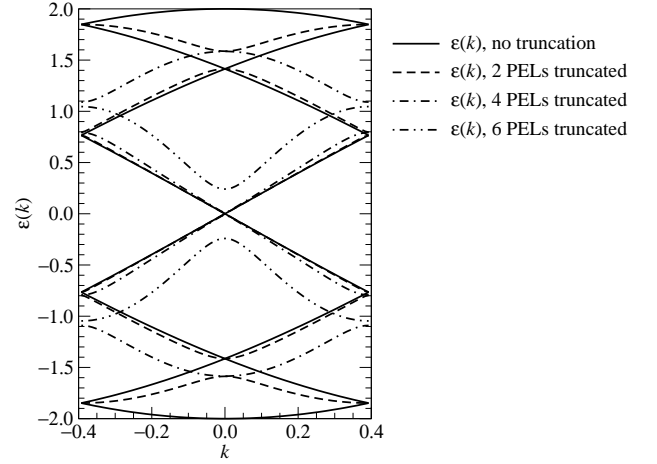


FIG. 12: Dispersion relation  $\epsilon(k)$  for a block of  $B = 8$  sites, where the effects of truncating 2, 4 and 6 PELs are shown. For this block size, truncating 2, 4 and 6 PELs corresponds to fractions  $\gamma = 0.75$ ,  $0.50$  and  $0.25$  of PELs retained. For  $\gamma = 0.75$ , the energy bands (dashed curves) just below and above the Fermi level  $\epsilon_F = 0$  agree with the true dispersion relation (solid curve) so well that the difference is not discernible at the scales presented in the figure.

In FIG. 12, we show the general features of the disper-

sion relation  $\epsilon(k)$  calculated within the operator-based truncation scheme, using the example of a block of  $B = 8$  sites. Apart from the energy gap  $\Delta E$  that opens up at the Fermi level  $\epsilon_F = 0$ , we see that there is a one-to-one correspondence between the PEL truncated and the energy band absent from the dispersion relation. More precisely, if we order the energy bands and the PELs from the lowest to the highest as  $\{\epsilon_1(k), \dots, \epsilon_B(k)\}$  and  $\{\varphi_1, \dots, \varphi_B\}$ , then if we truncate PEL  $\varphi_l$ , the energy band  $\epsilon_l(k)$  will also be removed from the numerically calculated dispersion relation. For fixed  $\gamma$ , the gap  $\Delta E$  decays exponentially with block size  $B$ , as is shown in FIG. 13, i.e. we have

$$\Delta E = \Delta E_0 \exp(-\kappa(\gamma)B), \quad (6.1)$$

where  $\kappa(\gamma)$  is an attenuation coefficient whose  $\gamma$ -dependence is shown in FIG. 14. Here we see also that  $\Delta E(B, \gamma)$  for different  $\gamma$  appears to converge onto  $\Delta E_0 \equiv \Delta E(B = 0)$ . Of course, there is no physical sense in talking about a block of zero size, but it is nevertheless a useful number to keep in mind when studying the scaling behaviour of  $\Delta E(B, \gamma)$  as  $\gamma$  varies.  $\Delta E_0$  is approximately 4, which is the bandwidth of the exact dispersion relation, in all cases.

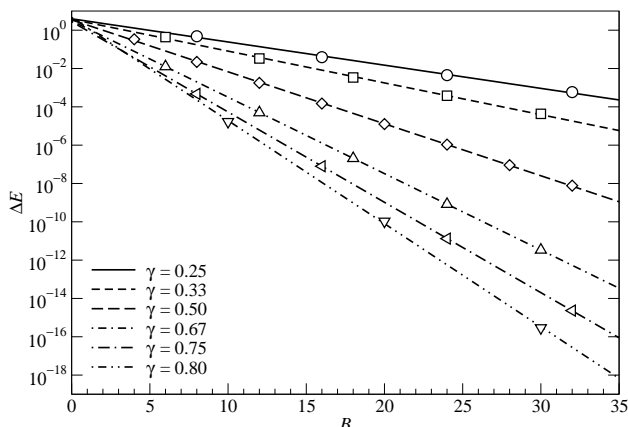


FIG. 13: Plot of the gap  $\Delta E$  as a function of block size  $B$  for various constant fractions  $\gamma = 1/4, 1/3, 1/2, 2/3, 3/4, 4/5$  of PELs retained. Also shown are fits to the data points for various  $\gamma$  to  $\Delta E(\gamma, B) = \Delta E_0 \exp(-\kappa(\gamma)B)$ .

In particular, in the limit of  $\gamma \rightarrow 1$ , where all PELs are retained, the gap is exactly zero for all nonzero block sizes  $B$ . In this limit, if we start out at a ‘gap’ of  $\Delta E_0$  at a ‘block size’ of  $B = 0$ , then to have  $\Delta E = 0$  at  $B = 1$ , we need the attenuation coefficient  $\kappa$  to be infinite, i.e. we expect the limiting behaviour  $\lim_{\gamma \rightarrow 1} \kappa(\gamma) = \infty$ . On the other hand, in the limit of  $\gamma \rightarrow 0$ , where we retain none of the PELs, it is again physically meaningless to talk of a dispersion relation. Nevertheless, if we pretend that we are able to calculate a ‘dispersion relation’ in this limit, then it is reasonable, following the trend observed in FIG. 13, that the gap never closes, i.e. we expect the

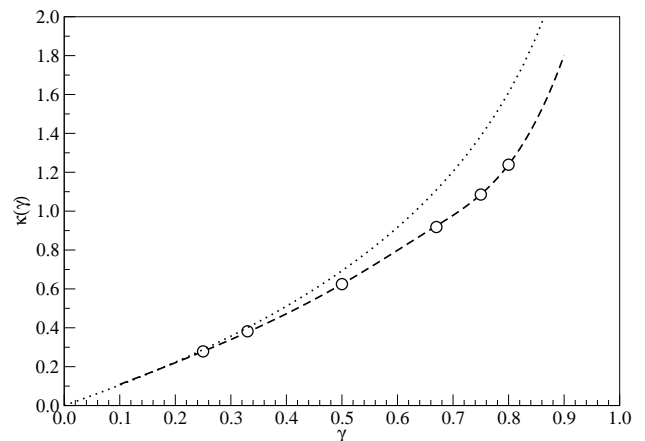


FIG. 14: Plot of the attenuation coefficient  $\kappa(\gamma)$  with which the spurious gap  $\Delta E$  decays, as a function of the fraction  $\gamma$  of PELs retained. A cubic spline curve (dashed curve) is superimposed on the data points to aid visualization. Also shown (dotted curve) is  $-\log_e(1 - \gamma)$ .

limiting behaviour  $\lim_{\gamma \rightarrow 0} \kappa(\gamma) = 0$ . These limiting behaviours appear to be borne out in the trend observed in FIG. 14.

Another notable feature in FIG. 14 is the fact that  $\kappa(\gamma) \approx \gamma$  for  $\gamma \ll 1$ , which is the regime we are most interested to apply the operator-based truncation scheme in. To appreciate the relevance of this observation, let us first note from FIG. 12 the general feature that the smaller the gap  $\Delta E$ , the better the truncated dispersion relation about the Fermi level. From (4.32) we saw that the truncated weight  $W_t$  depends only on the combination  $l_{\max} = \gamma B$  in this regime, and as far as  $W_t$  is concerned, there is no difference whether we choose to keep 10 out of 100 PELs ( $\gamma = 0.1$ ) or 10 out of 200 PELs ( $\gamma = 0.05$ ). Here we see a similar exponential dependence on  $l_{\max}$  for the spurious gap  $\Delta E$  that arises due to truncation: if we write  $\kappa \approx \gamma$  in this regime, then  $\Delta E \approx \Delta E_0 \exp(-B\gamma) = \Delta E_0 \exp(-l_{\max})$ . Such an exponential behaviour implies that we have very good control over the numerical accuracy of the dispersion relations — in particular near the Fermi level — calculated in the operator-based DM truncation scheme.

## B. Fermi Velocity

When the block size  $B$  is odd, the central energy band crosses the Fermi level, and the quantity of interest becomes the Fermi velocity  $v_F$ . This can be determined from the truncated dispersion relation by taking the numerical central derivative of the central energy band at  $k = \pm \bar{n}\pi/B$ . At half-filling,  $\epsilon(k = \pm \pi/2B) = 0$  exactly because of particle-hole symmetry. This feature of the dispersion relation was found to be preserved in

the numerical dispersion relations computed within the operator-based DM truncation scheme. On the global scale, we find numerically that the shifts in the central energy band at the Brillouin zone center and Brillouin zone edge are such that  $v_F > 2$  always. However, when  $B$  is large, the numerical diagonalization routine introduces artefacts on the energy scale of  $10^{-13}$ , resulting in the locally evaluated  $v_F$  coming out to be very slightly less than 2. As such, we analyze the behaviour of  $v_F$  as a function of  $B$  and  $\gamma$  only for  $B < 150$ , as shown in FIG. 15.

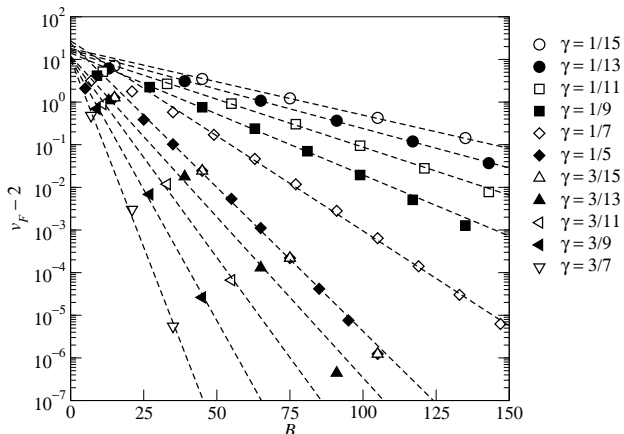


FIG. 15: Plot of Fermi velocity deviation ( $v_F - 2$ ) calculated from the truncated dispersion relation, as a function of the block size  $B$ , for various fractions  $\gamma = 1/15, 1/13, 1/11, 1/9, 1/7, 1/5, 3/15, 3/13, 3/11, 3/9, 3/7$  of PELs retained. Fits to average exponential decays are also shown.

As can be seen from FIG. 15, the difference ( $v_F - 2$ ) decays more or less exponentially with  $B$  for various  $\gamma$ , i.e.

$$(v_F - 2) \cong \exp(-\xi(\gamma)B), \quad (6.2)$$

where  $\xi(\gamma)$  is the  $\gamma$ -dependent attenuation coefficient for the average exponential decay. The  $\gamma$ -dependence of  $\xi(\gamma)$  is shown in FIG. 16.

### C. Real-Space Structure of Eigenfunctions of Truncated Hamiltonian

The eigenfunctions of the untruncated Hamiltonian (1.1) are spatially uniform plane waves, with amplitude  $\exp(ikj)/\sqrt{B}$  on site  $j$  of the block of  $B$  sites. These can be expanded in terms of the density matrix eigenfunctions  $\chi_l(j, B)$ . Naively, we expect that if we drop those  $\chi_l(j, B)$  associated with pseudo-energies  $\varphi(l, B)$  far from the pseudo-Fermi level  $\varphi_F$ , as we would in our operator-based truncation scheme which removes these single-particle pseudo-energy levels as degrees of freedom, the remaining terms, all having enhanced amplitudes at

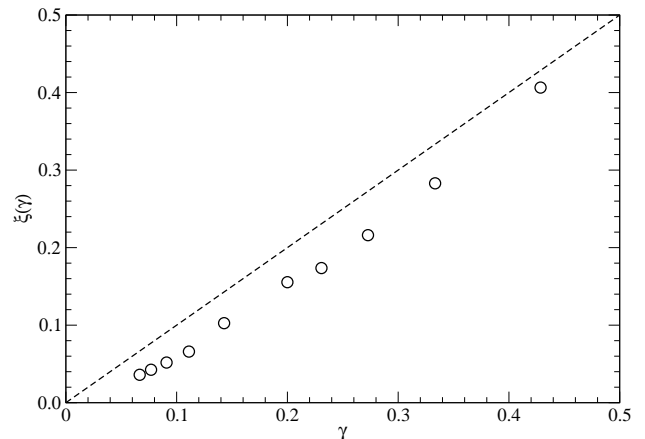


FIG. 16: Plot of the attenuation coefficient  $\xi(\gamma)$  as a function of the fraction  $\gamma$  of PELs retained. Also shown (dashed line) is the expected behaviour  $\xi(\gamma) = \gamma$ .

the edge of the block, would sum to a function with enhanced amplitude at the edge of the block. It would therefore seem like we are attempting to approximate a spatially-uniform plane wave with a function with the wrong real-space structure.

However, the key insight we gain from our study of block density matrices is that while the system-wide density matrix  $\rho_0$  commutes with  $H$  in (1.1), the block density matrix  $\rho_B$  obtained by tracing down  $\rho_0$  does not commute with  $H(k)$ , for all  $k$ . Therefore, after operator-based truncation  $H(k) \rightarrow \tilde{H}(k)$ , we would need to diagonalize  $\tilde{H}(k)$  to find the truncated dispersion relation  $\epsilon_l(k)$ . Thus, the function that would approximate the plane wave is not the latter's truncated expansion in terms of the eigenfunction of the one-particle block density matrix, but rather, a particular eigenfunction of  $\tilde{H}(k)$ , which is an appropriate linear combination of the  $\chi_l(j, B)$  retained in the operator-based truncation scheme. We show in FIG. 17 the spatial structure of such a function, for various numbers of density matrix eigenfunctions retained. As we can see, for a block of  $B = 23$  sites, keeping 7 density matrix eigenfunctions with pseudo-energies around  $\varphi_F$  would produce a decent approximation to the plane wave with  $k = \pi/2B$ .

### D. Discussion

We speculate that the fact that the operator-based density matrix truncation scheme succeeds so well suggests that appropriate linear combinations of the density matrix eigenfunctions can closely approximate a plane wave with wavevector  $\pm k_F$ . This is only possible by taking the difference of two eigenfunctions so as to cancel the enhancements of the envelope function seen at the block ends (see Section V). Indeed, the fact that we get the correct slope  $v_F$  of the dispersion near  $k_F$  suggests

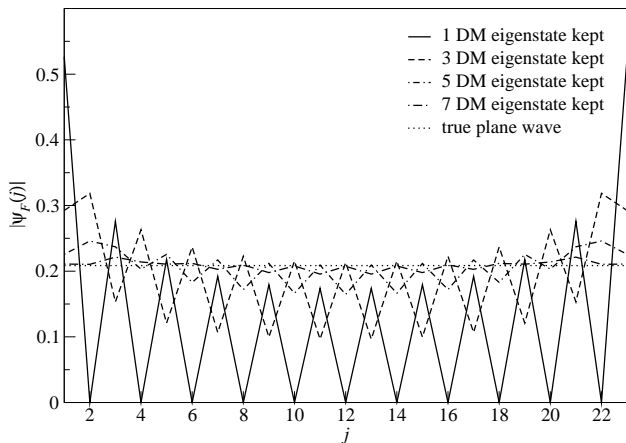


FIG. 17: Amplitudes of eigenfunctions of the truncated Hamiltonian  $\hat{H}(k_F)$  for different numbers of PELs retained, for a block of  $B = 23$  sites at half-filling.

that by taking different weights, a continuously varying effective wavevector can be approximated.

The fact that the goodness of approximation depends only on the number of eigenfunctions kept, means that we approximate the wavefunction about as well in two successive blocks of  $B$  sites, as we do in one big block of  $2B$  sites. One could speculate that there might exist some sort of approximate composition formula, analogous to Clebsch-Gordan formulas for combining angular momenta, that provides the  $2B$ -site eigenfunctions in terms of the direct product of the  $B$ -site eigenfunctions.

## VII. OPERATOR-BASED PLANE WAVE TRUNCATION SCHEME

As we saw in Section V, eigenstates of the density matrix  $\rho_B$  are approximately plane waves (with wavevector  $Q$  determined by the boundary conditions on the block of  $B$  sites) modified by some envelope function. Apart from the effects of the envelope functions, the operator-based truncation scheme described above is likened to truncating wavevectors  $Q$  far away from the Fermi wavevector  $k_F$ . It is therefore natural to investigate how an operator-based truncation scheme based on plane waves would fare against that based on the density matrix eigenstates.

### A. Exact Dispersion at Zone Center

Compared to the *operator-based DM truncation scheme* developed above, the most striking feature of the *operator-based plane wave (PW) truncation scheme* is that it gets the dispersion exactly right at the zone center, as shown for the case of  $B = 8$  in FIG. 18, and for the case of  $B = 10$  in FIG. 19. We understand this as follows:

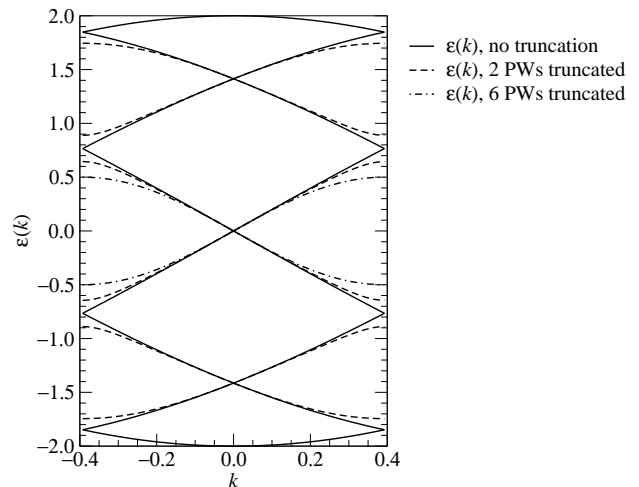


FIG. 18: Dispersion relation  $\epsilon(k)$  for a block of  $B = 8$  sites, where the effect of truncating 2 and 6 plane waves (PWs) are shown. For  $B = 4n$ , the Fermi level is located at the zone center, and  $\epsilon(k)$  is always gapless here regardless of the number of plane waves truncated.

To evaluate the dispersion relation in a blocked description, we start by defining the direct Bloch basis states

$$|j, k\rangle = \frac{1}{\sqrt{N/B}} \sum_J e^{ikJB} |j, J\rangle, \quad j = 1, \dots, B, \quad (7.1)$$

where  $|j, J\rangle = c_{j+JB}^\dagger |0\rangle$  is the single-particle occupation number basis state at site  $j + JB$  along the chain. In this basis, the Hamiltonian (1.1) for a chain of  $N$  non-interacting spinless fermions take on a block diagonal form. Diagonalizing the  $B \times B$  diagonal block

$$H(k) = \begin{bmatrix} 0 & -1 & 0 & \dots & -e^{-ikJB} \\ -1 & 0 & -1 & \dots & 0 \\ 0 & -1 & 0 & \dots & 0 \\ \vdots & & & \ddots & \vdots \\ -e^{ikJB} & 0 & 0 & \dots & 0 \end{bmatrix} \quad (7.2)$$

for  $-\pi/B \leq k < \pi/B$  then gives the dispersion relation within the reduced zone scheme.

For the operator-based PW truncation scheme, we need to work with the plane wave states  $|Q, J\rangle$  on each block of  $B$  sites, where the wavevector  $Q$  is determined by periodic boundary condition, i.e.  $\exp(iQB) = 1$ . These plane wave states are related to the single-particle occupation number basis states by

$$|Q, J\rangle = \frac{1}{\sqrt{B}} \sum_{j=1}^B e^{iQj} |j, J\rangle. \quad (7.3)$$

A Bloch basis state parallel to (7.1) can be defined as

$$|Q, k\rangle = \frac{1}{\sqrt{N/B}} \sum_J e^{ikJB} |Q, J\rangle, \quad (7.4)$$



where  $QB/2\pi = 0, \dots, B-1$ . From (7.3) and (7.4), it is easy to see that

$$|Q, k\rangle = \frac{1}{\sqrt{B}} \sum_{j=1}^B e^{iQj} |j, k\rangle. \quad (7.5)$$

At the zone center,  $k = 0$ , and the  $B \times B$  Hamiltonian matrix in the  $|j, k\rangle$  basis that we need to diagonalize becomes

$$H(0) = \begin{bmatrix} 0 & -1 & 0 & \cdots & -1 \\ -1 & 0 & -1 & \cdots & 0 \\ 0 & -1 & 0 & \cdots & 0 \\ \vdots & \vdots & \vdots & \ddots & \vdots \\ -1 & 0 & 0 & \cdots & 0 \end{bmatrix}. \quad (7.6)$$

It is trivial to check that the eigenstates of this Hamiltonian matrix are precisely the plane waves  $|Q, 0\rangle$  on the block. Therefore, in the  $|Q, k\rangle$  basis,  $H(k)$  is diagonal at  $k = 0$ , and so truncating some plane waves from the Hilbert space produces no effect on the dispersion here.

To be more precise, in performing truncation, a linear subspace of the Hilbert space is chosen, and the Hamiltonian projected onto this subspace. If  $|\psi\rangle$  is an eigenstate of the full Hamiltonian, and if  $|\psi\rangle$  is retained in the truncated Hilbert space, then it will continue to be an eigenstate of the truncated Hamiltonian, with the same eigenvalue.

### B. Energy Gap at Zone Boundary

For even block sizes with  $B = 4n$ , the Fermi level is located at the zone center in the reduced zone scheme, and so there is no energy gap to speak of. On the other hand, for even block sizes with  $B = 4n+2$ , the Fermi level is located at the zone boundary. At the zone boundary, operator-based PW truncation introduces an energy gap  $\Delta E$  at the Fermi level, as shown in FIG. 19 for  $B = 10$ .

As in the case for the operator-based DM truncation scheme, we investigate the behaviour of the energy gap  $\Delta E$  as a function of the block size  $B$  for a fixed fraction  $(1 - \gamma)$  of block states truncated. However, for the operator-based PW truncation scheme, the number of plane wave states that can be truncated, if  $B$  is even, is  $4m + 2$ ,  $m = 0, 1, 2, \dots$ . Thus the only realizable series of block sizes  $B$  on which we can perform fixed  $(1 - \gamma)$  truncation are of the form  $B = q(4m + 2)$ ,  $q = 2, 3, \dots$ . The fraction  $\gamma$  of block plane wave states retained is related to the series index  $q$  by

$$\gamma = 1 - \frac{1}{q}. \quad (7.7)$$

Half of these realizable series have block sizes that are multiples of 4, for which the Fermi level is at the Brillouin zone center where the dispersion relation we have

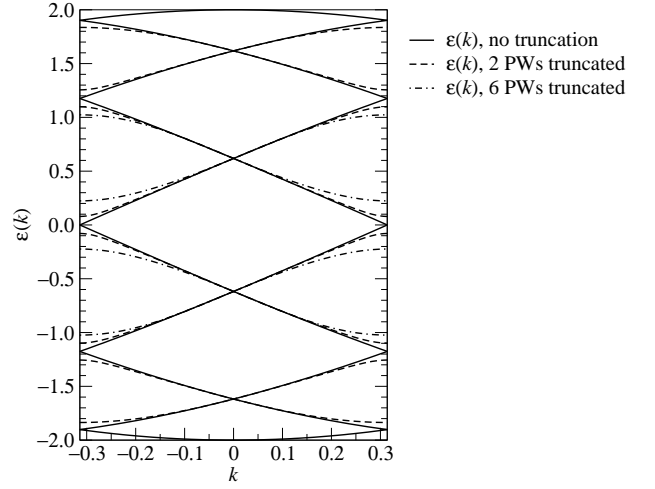


FIG. 19: Dispersion relation  $\epsilon(k)$  for a block of  $B = 10$  sites, where the effect of truncating 2 and 6 plane waves (PWs) are shown. For  $B = 4n + 2$ , the Fermi level is located at the zone boundary, and the operator-based plane wave truncation scheme introduces an energy gap  $\Delta E$  here.

shown in the previous subsection to be gapless. In this subsection we are interested in those block sizes for which  $q$  is an odd integer, since for these block sizes the Fermi level is at the Brillouin zone boundary, where a gap develops in the dispersion relation as a result of truncation. The behaviour of  $\Delta E$  as a function of  $B$  for three series of  $q$  is shown in FIG. 20.

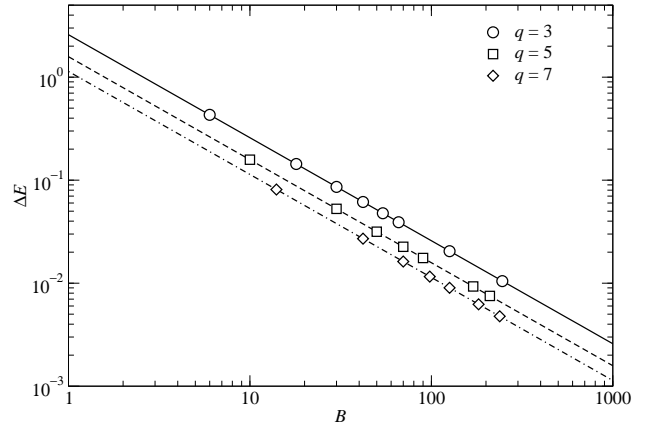


FIG. 20: Plot of  $\Delta E$  as a function of block size  $B$  for  $q = 3, 5$  and  $9$ , corresponding to the fractions  $\gamma = 2/3, 4/5, 6/7$  of block plane wave states retained. Also shown are the fits of the data points to the formula  $\Delta E(B, \gamma) = \Delta E_1(\gamma)/B$ . From the fits, we have  $\Delta E_1 = 2.58263$  for  $\gamma = 2/3$ ,  $\Delta E_1 = 1.57991$  for  $\gamma = 4/5$  and  $\Delta E_1 = 1.13532$  for  $\gamma = 6/7$ .

As can be seen from FIG. 20, the gap depends on block size as an inverse power law

$$\Delta E(B, \gamma) = \frac{\Delta E_1(\gamma)}{B}, \quad (7.8)$$

where  $\Delta E_1(\gamma)$  is a  $\gamma$ -dependent prefactor. This is in stark contrast to the exponential dependence (6.1) found for the case of the operator-based density matrix truncation scheme.

### C. Fermi Velocity

For odd  $B$ , we again investigate the behaviour of  $v_F$  as a function of  $B$  for the operator-based plane wave truncation scheme. The number of block plane waves that can be truncated is  $4m + 3$ ,  $m = 0, 1, 2, \dots$  and the series of realizable block sizes are  $B = q(4m + 3)$ ,  $q = 3, 5, \dots$ . Unlike in the operator-based DM truncation scheme, there appears to be two different systematic behaviours for  $v_F(B, \gamma)$ , one for  $q = 4p - 1$  and another for  $q = 4p + 1$  ( $p = 1, 2, \dots$ ). We find that the Fermi velocity can be fitted very well to the formula

$$v_F = \begin{cases} \bar{v}_F(\gamma) + c_+(\gamma)/B, & q = 4p - 1; \\ \bar{v}_F(\gamma) - c_-(\gamma)/B, & q = 4p + 1. \end{cases} \quad (7.9)$$

The plots of  $\bar{v}_F(\gamma)$  and  $c_{\pm}(\gamma)$  as a function of  $\gamma$  are shown in FIG. 21 and FIG. 22 respectively.

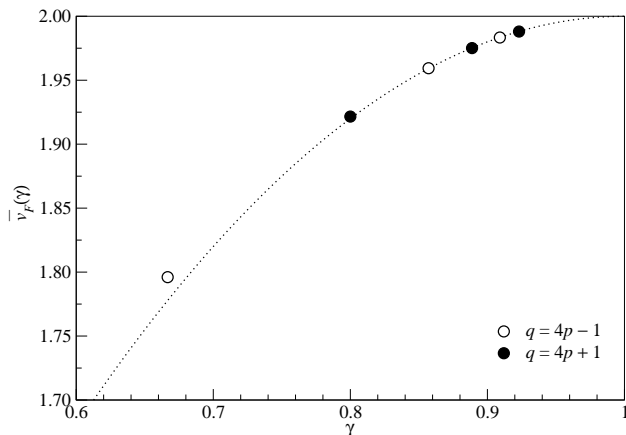


FIG. 21: Plot of  $\bar{v}_F$  as a function of  $\gamma$  in the operator-based PW truncation scheme for both the  $q = 4p - 1$  series and  $q = 4p + 1$  series. Also shown as the dashed curve is  $2[1 - (1 - \gamma)^2]$ , which appears to fit the data points well near  $\gamma = 1$ .

As can be seen from FIG. 21, the exact value of the Fermi velocity is obtained only in the double limit of  $B \rightarrow \infty$  and  $\gamma \rightarrow 1$ . Compared to the operator-based DM truncation scheme, where we manage to achieve the exact Fermi velocity for any  $\gamma$ , this is clearly undesirable. Furthermore, even very close to  $\gamma = 1$ , the computed Fermi velocity approaches the limiting value  $\bar{v}_F(\gamma)$  as  $B^{-1}$ . This is much slower than the exponential convergence of  $\exp(-\xi(\gamma)B)$  found for the operator-based DM truncation scheme.

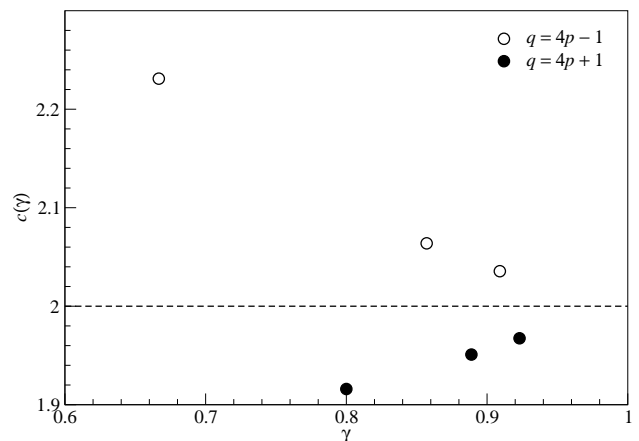


FIG. 22: Plot of  $c_{\pm}$  as a function of  $\gamma$  in the operator-based PW truncation scheme for both the  $q = 4p - 1$  series ( $c_+(\gamma)$ ) and  $q = 4p + 1$  ( $c_-(\gamma)$ ) series. Both  $c_+(\gamma)$  and  $c_-(\gamma)$  appears to be converging towards 2. In fact, from the graph we find that  $|c_{\pm}(\gamma) - 2| \approx 0.43(1 - \gamma)$ .

## VIII. SUMMARY AND DISCUSSIONS

### A. Statistical-Mechanical Analogy and Scaling

To summarize, we have in this paper developed an in-depth understanding of the structure of the eigenvalues and eigenstates of the density matrix  $\rho_B$  of a block of  $B$  sites embedded within a infinite one-dimensional chain of noninteracting spinless fermions described by the set of fermion operators  $\{\tilde{c}_k\}$  with dispersion relation  $\epsilon(k)$ .

From Ref.7 we know that the block density matrix  $\rho_B$  can be written in (1.2) as the exponential of a pseudo-Hamiltonian  $\tilde{H}$  given by (1.3) acting only within the block, which describes another system of noninteracting spinless fermions with fermion operators  $\{f_l\}_{l=1}^B$  and dispersion relation  $\varphi_l$ . We use the prefix *pseudo*- when talking about operators  $\{f_l\}_{l=1}^B$  and energies  $\varphi_l$  to distinguish them from the operators  $\{\tilde{c}_k\}$  and energies  $\epsilon(k)$  of the system we started out with.

The many-particle eigenstates of  $\rho_B$  can then be interpreted simply as the many-body energy eigenstates (2.1) of the system of noninteracting spinless fermions described by  $\tilde{H}$ , and their associated density matrix weights (2.2) are then their statistical weights in the grand canonical ensemble, *as though* the block is at a finite temperature. Within this statistical-mechanical picture, we can apply intuitions learnt from the statistical mechanics of real fermionic systems, and talk about the filling of single-particle pseudo-energy levels (PELs) as dictated by the Fermi-Dirac distribution, the pseudo-Fermi sea with its pseudo-Fermi level  $\varphi_F$  and particle-hole excitations of the pseudo-Fermi sea.

Using results obtained in Ref.7, we make this statistical-mechanical picture more precise, by identifying the single-particle eigenstates  $|\chi_l\rangle$  in (2.6) of  $\rho_B$

as those built up from the eigenvectors  $\{\chi_l(j)\}$ ,  $j = 1, \dots, B$ , of the Green function matrix  $G$  restricted to the block. The eigenvalue  $\lambda_l$  of  $G$ , related to the single-particle pseudo-energies  $\varphi_l$  by (2.7) and (2.8), are the average pseudo-occupation numbers of the  $l^{\text{th}}$  PEL.

The statistical mechanics of real fermionic systems tells us that, at finite temperature, the physically important many-body states are those low-energy particle-hole excitations involving single-particle energy levels within  $k_B T$  of the Fermi level. Single-particle energy levels far away from the Fermi level contribute negligibly to the thermodynamic properties of the fermionic system, and are precisely the degrees of freedom to be truncated in a renormalization group analysis.

We capitalize on this insight, and described a recipe for operator-based truncation of the density matrix eigenstates, where out of the  $B$  pseudo-fermion operators  $\{f_l\}_{l=1}^B$ , we truncate those  $f_l$ 's associated with single-particle pseudo-energies  $\varphi_l$  far away from  $\varphi_F$  and retain  $l_{\text{max}}$  of them with  $\varphi_l \approx \varphi_F$ . Within this operator-based truncation scheme, the effective pseudo-Hamiltonian acting on the truncated Hilbert space can be made to have the same form as the original pseudo-Hamiltonian, in the same spirit of renormalization group transformations in statistical mechanics or quantum field theory.

Having laid out the basic principles behind our operator-based DM truncation scheme, we proceeded to look more closely into the distribution of single-particle pseudo-energies  $\varphi_l$ , and how these scale with the block size  $B$ . There are two related questions that provide the motivation for doing this: (1) the statistical mechanics of real fermionic systems suggests that single-particle energy levels within  $\beta^{-1} = k_B T$  of the Fermi level are the physically relevant degrees of freedom — what then is the effective temperature  $\tilde{\beta}^{-1}$  that we should use as the natural cutoff when performing operator-based truncation on  $\{f_l\}_{l=1}^B$ ? (2) although we have associated the pseudo-dispersion relation  $\varphi_l$  with the dispersion relation  $\epsilon(k)$  of a real fermionic system of noninteracting spinless fermions, the wavevector  $k$  enumerating  $\epsilon(k)$  is an *intensive* quantity whereas the ordinal number  $l$  enumerating  $\varphi_l$  is an *extensive* quantity — what would the intensive analog of  $l$  that more closely parallels the wavevector  $k$ , and how would the pseudo-dispersion relation look like in terms of this intensive label?

The natural answer to the second question would be to write the pseudo-dispersion relation  $\varphi_l$  as a function of  $l/B$ , totally analogous with how the wavevector  $k$  is enumerated as  $2\pi m/N$  for a chain of  $N$  sites satisfying the Born-von Karman boundary condition. In fact, we find strong numerical evidence that suggests that the single-particle pseudo-energies, for various block sizes and fillings, satisfy a scaling relation of the form given in (3.6), where the scaling function  $f(\bar{n}, x)$  is the proper analog of the dispersion relation  $\epsilon(k)$ , and the scaling variable  $x$  given in (3.7) is the proper analog of the wavevector  $k$ . From (3.12), we see that the block size  $B$  plays the role

of inverse temperature.

Our scaling results in Section III indicate that the density matrix eigenstates and eigenvalues behave, as block size  $B$  is increased, very much as energy eigenstates and eigenvalues do when the system size is increased. In the latter case, we have a dispersion relation and are more or less sampling it at different wavevectors. It is not quite that simple in the density matrix case, since the scaling function (3.6) — our analog of the energy dispersion relation — depends on the filling  $\bar{n}$ . We only note that this analogy still lacks an analytical foundation. A more penetrating analysis is called for of the relation of  $G$  to  $\rho_B$  (or equivalently, the effect on its eigenvalues of restricting  $G$  to sites on a block).

Incidentally, we noted that our equation relating  $G$  to  $\rho_B$  was valid at any temperature, but we assumed zero temperature throughout this paper. We expect nonzero temperature  $T$  would become a second scaling variable. Since  $T > 0$  has similar effects on the Green function  $G(r)$  as does the gap introduced in (4.5), we expect the scaling also behaves similarly and we did not investigate it.

## B. Scaling as a Guide to Truncation in Practice

In a real application, it appears quite unlikely that Hamiltonians will be projected directly onto large blocks (meaning blocks of more than 16 sites). What then is the practical value of extracting scaling forms, if they are unambiguously seen only in blocks of 100 or more sites? One answer is that, even though it is an oversimplified cartoon for the non-asymptotic situations in which it usually gets applied, a scaling law is easier to grasp than brute numerical or graphical facts.

The scaling relation (3.6) is a powerful tool that we can use to derive deeper understanding concerning the structure of the block density matrix, as well as various aspects of truncation. But in itself, the scaling relation provides only a partial answer to our first question, which is about how much of the Hilbert space of many-body states on the block of  $B$  sites we can truncate. To answer this question more completely, we looked at the three density matrix eigenstates  $|F\rangle$ ,  $|F-1\rangle$  and  $|F+1\rangle$  with the largest weights. Using the scaling relation (3.6), we find that the ratios  $w_{F\pm 1}/w_F$  of their weights ( $w_F$  being the largest density matrix weight) approach a constant, in (4.4) for a gapless system of noninteracting spinless fermions, as  $B \rightarrow \infty$ .

The same result was also found for a gapped system of noninteracting spinless fermions, for which we find scaling relations governed by gap-dependent scaling functions. Furthermore, the scaling relation (3.6) allowed us to conclude that as  $B \rightarrow \infty$ , the largest density matrix weight  $w_F$  approaches a constant given in (4.19), and derive approximately the dependence on the number  $l_{\text{max}}$  of PELs retained and the truncated weight  $W_l$  in the

operator-based DM truncation scheme.

### C. DMRG and Operator-Based Truncation

It is difficult to compare our results with those obtained in the context of the DMRG, because that is an incremental method. Rather than obtain the density matrix of a large block all at once, each iteration of the DMRG takes an approximate density matrix for a block of  $B$  sites and produces an approximate density matrix for a block of  $(B + 1)$  sites. The fraction of weight kept, which is taken as the figure of merit, refers to the small truncation in each iteration. The cumulative DMRG truncation might be more appropriate to compare with our results for rather large blocks.

Nevertheless, let us note that operator-based truncation can be applied independent of whether we use an incremental or one-shot method. In particular, operator-based truncation could be used in a test run to apply DMRG to a noninteracting Fermi chain. One is given a truncated list of  $t$  operators  $\{f_l\}$  where  $l = (B - t + 1)/2, \dots, (B + a - 1)/2$  for the original block, and a Hamiltonian projected onto it. One augments this list with the bare creation operators  $c_{B+1}^\dagger$  on a new site that will be added, and defines the new Hamiltonian by adding the hopping to the new site.

In light of the derivation of Ref.7, we anticipate that the density matrix of the augmented system's ground state must have the same quadratic form, with new operators  $\{f'_l\}$ , which could presumably be obtained merely by diagonalizing the single-particle sector. One simply deletes the least important member of this list to obtain a new truncated list, no longer than the original one.

This difficulty notwithstanding, we still carried out a naive comparison of the performance of the operator-based DM truncation scheme against the traditional weight-ranked DM truncation scheme used in the DMRG, using the ability to exhaust the sum rule (4.1) for a given total number  $L_{\max}$  of density matrix eigenstates retained as a criterion. The conclusion: while the operator-based DM truncation scheme do not exhaust the sum rule (4.1) as rapidly as the weight-ranked DM truncation scheme,  $W_t$  is still of  $O(1)$ , i.e. the significant parts of the total density matrix weight are 'captured' by the operator-base DM truncation scheme.

#### 1. Truncation and Dispersion Relations

However, we believe it is more important to check how well a truncation scheme do by calculating physical quantities, rather than rely solely on the truncated weight  $W_t$  as a performance indicator. To this end, we calculated the dispersion relation of elementary excitations within the operator-based DM truncation scheme (an easy thing

to do), and found that the error incurred decays exponentially as  $l_{\max}$ , the number of PELs retained when  $l_{\max} \ll B$ . This error is much smaller than  $O(\epsilon)$ , which is expected from a naive analysis based on the discarded weight  $\epsilon = 1 - W_t$ . Here, there is subtle worry that it may be that truncation works especially well for our chosen hopping Hamiltonian (1.1) is so local. A Hamiltonian with longer range hopping would have the same Fermi sea and hence the same density matrix, but the truncation errors might be worse.

It would be desirable to also calculate the dispersion relation within the weight-ranked DM truncation scheme, and compare the results to those obtained within the operator-based DM truncation scheme. However, in the latter case it is problematic even to define the question, since each retained density matrix eigenstate would be a many-particle state. The new truncated Hamiltonian might be conveniently expressed in terms of the pseudo-creation operators  $\{f_l\}$ , but many combinations of occupations would not exist.

The situation would be somewhat analogous to taking a simple, noninteracting hopping Hamiltonian for spinfull fermions, and imposing a Gutzwiller projection (no doubly occupied sites). In effect, the projection made a noninteracting model into an interacting one. Similarly a weight-ranked truncation must introduce spurious interactions. Hence, even if a system containing several blocks were to be exactly diagonalized (using the truncated basis) we could not immediately identify the elementary excitations. One would need, for example, to numerically compute a spectral function  $S(q, \omega)$ , where  $(\hbar q, \hbar \omega)$  are momentum and energy, and then locate peaks as a function of  $\hbar \omega$ . On the other hand, a system which is truncated using the operator-based truncation scheme can still be represented by a set of creation and annihilation operators.

#### 2. Inadequacy of Plane-Wave Truncation Scheme

Following this, we argued, based on the real-space structure of the one-particle density matrix eigenfunctions shown in Section V, that an operator-based truncation scheme can also be defined naturally using the basis formed by single-particle plane wave (PW) states on the block of  $B$  sites. The dispersion relation was calculated within this operator-based PW truncation scheme, and compared to that calculated within the operator-based DM truncation scheme. We find that, other than getting the dispersion exactly right at the zone center of the reduced Brillouin zone, the operator-based PW truncation scheme is generally inferior to the operator-based DM truncation. Instead of decaying exponentially as  $l_{\max}$ , the error in the dispersion relation calculated within the operator-based PW truncation scheme decays as a power law  $l_{\max}^{-1}$ , which means that more single-particle basis states need to be retained in the operator-based PW

truncation scheme as compared to the operator-based DM truncation scheme.

#### D. Towards Interacting Systems in Dimensions $d \geq 2$

It is not much harder in principle to analyze the proposed operator-based density matrix truncation scheme for *noninteracting* fermions in two dimensions. However, it will be harder to understand the scaling since we cannot simply rank the eigenvalues. One dimension was special because we know that each successive state has one more node than the previous one. A further very important difference is that in  $d = 1$  there are just two Fermi points, whereas in  $d \geq 2$  there is a Fermi surface. Thus, whereas in  $d = 1$  the density matrix eigenstates near the pseudo-Fermi level are related to the energy eigenstates at  $\pm k_F$ , in  $d \geq 2$  these eigenstates will correspond to mixtures of wavevectors from every piece of the Fermi surface.

Obviously, noninteracting systems do not require numerical studies, so we must clarify how our results are relevant to the problem of interacting systems. Firstly, many (gapless) systems of interest are in a phase — Fermi liquid,  $d$ -wave superconductor — which are noninteracting in the low-energy, long-wavelength limit. When applied to a Fermi liquid system, we expect (to the extent that the truncation has separated out the low energy modes) that any iterative renormalization scheme will converge on the noninteracting limit, and it must behave properly in that limit to have even the hope of success. Hence, for a density matrix-based scheme, the first order of business is to study the density matrix for a free fermion ground state (as in this paper) or for a BCS state,<sup>8</sup> i.e. that the density matrix will actually have the simple operator-based form, and hence its many-particle eigenstates of the density matrix really are built from the single-particle eigenstates.

For an interacting system, the truncated basis should of course be constructed using the many-body density matrix for that system (not the noninteracting system). We expect that the operators generating this many-particle truncated basis will *not* just be those that cre-

ate the 1-particle density matrix eigenstates (they were in the noninteracting case studied in this paper). More thought will be needed as to discover the best recipe to optimize the truncation rule so as to balance the needs of sectors with different particle numbers in a strongly interacting system. The simple algebraic structure of the noninteracting density matrix eigenstates, considered in this paper, has motivated investigations (in progress) of the relationships among the many-particle density matrix eigenstates for an interacting system.

A separate reason why our results for the noninteracting fermions are relevant to the study of interacting systems is that the scaling behaviour of the noninteracting density matrix should be a good guide to that of interacting systems, although details may differ. This is in the same sense that mean-field theory is a good guide to the overall pattern of critical phenomena.

However, other interacting models of interest sit at quantum critical points that are not described by quasiparticle interactions, or possess fractionalized excitations. Since we do not presently understand the proper way to write their wavefunctions in terms of a spatially blocked basis, nor the proper renormalization step to capture the interblock correlations in the fractionalized systems, we do not know if a plain block density matrix gives the proper basis for truncation of the states. Furthermore, in the absence of an analytic construction of the block density matrix, for example, for Laughlin's quantum Hall wavefunction or the one-dimensional Su-Schrieffer state, we cannot proceed to scaling studies of large blocks like those found in the present paper, but numerical studies of such density matrices might be an illuminating subject for future research.

#### Acknowledgments

This research is supported by NSF grant DMR-9981744, and made use of the computing facility of the Cornell Center for Materials Research (CCMR) with support from the National Science Foundation Materials Research Science and Engineering Centers (MRSEC) program (DMR-0079992).

<sup>1</sup> S. R. White, Phys. Rev. Lett. **69**, 2863 (1992).

<sup>2</sup> S. R. White, Phys. Rev. B **48**, 10345 (1993).

<sup>3</sup> S. Östlund and S. Rommer, Phys. Rev. Lett. **75**, 3537 (1995).

<sup>4</sup> S. R. White, Phys. Rep. **301**, 187 (1998).

<sup>5</sup> R. M. Noack, S. R. White, and D. J. Scalapino, in *Computer Simulation Studies in Condensed Matter Physics VII (Proceedings of the Seventh Workshop, Athens, GA, USA, 28 February – 4 March 1994)*, edited by D. P. Landau, K.-K. Mon, and H.-B. Schüttler (Athens, Georgia, USA,

1994), pp. 85–98.

<sup>6</sup> S. Liang and H. Pang, Phys. Rev. B **49**, 9214 (1994).

<sup>7</sup> S.-A. Cheong and C. L. Henley, cond-mat/0206196 (2002).

<sup>8</sup> M. C. Chung and I. Peschel, Phys. Rev. B **64**, art. 064412 (2001).

<sup>9</sup> R. K. Pathria, *Statistical Mechanics, 2nd Edition* (Butterworth-Heinemann (Oxford), 1996).

<sup>10</sup> E. R. Davidson and L. L. Jones, J. Chem. Phys. **37**, 2966 (1962).

<sup>11</sup> C. F. Bender and E. R. Davidson, J. Chem. Phys. **70**, 2675

- (1966).
- <sup>12</sup> F. Jensen, *Introduction to Computational Chemistry* (John Wiley & Sons (Chichester), 1999).
- <sup>13</sup> P. W. Anderson, *J. Phys. C* **3**, 2436 (1970).
- <sup>14</sup> T. Xiang, *Phys. Rev. B* **53**, R10445 (1996).
- <sup>15</sup> J. Dukelsky and G. Sierra, *Phys. Rev. Lett.* **83**, 172 (1999).
- <sup>16</sup> F. Gebhard, K. Bott, M. Scheidler, P. Thomas, and S. W. Koch, *Phil. Mag. B* **75**, 1 (1997).
- <sup>17</sup> J. Gaité, *Mod. Phys. Lett.* **A16**, 1109 (2001).
- <sup>18</sup> *Octave*, URL <http://www.octave.org/>.
- <sup>19</sup> The same conclusion holds for the case of  $B$  odd, apart from the technical annoyance that there are *two* many-particle density matrix eigenstates with the largest weight.